Red Blood Cell Segmentation and Classification from Microscopic Images Using
Machine Learning

Mr. Korranat Naruenatthanaset

จุฬาลงกรณ์มหาวิทยาลัย
CHULALONGKORN UNIVERSITY

A Thesis Submitted in Partial Fulfillment of the Requirements
for the Degree of Master of Engineering in Computer Engineering
Department of Computer Engineering
FACULTY OF ENGINEERING
Chulalongkorn University
Academic Year 2020

การตัดแยกและจำแนกเม็ดเลือดแดงจากภาพถ่ายจากกล้องจุลทรรศน์ด้วยวิธีการเรียนรู้ของเครื่อง

นายกรณัฏฐ์ นฤนาทธนาเสฏฐ์

วิทยานิพนธ์นี้เป็นส่วนหนึ่งของการศึกษาตามหลักสูตรปริญญาวิศวกรรมศาสตรมหาบัณฑิต
สาขาวิชาวิศวกรรมคอมพิวเตอร์ ภาควิชาวิศวกรรมคอมพิวเตอร์
คณะวิศวกรรมศาสตร์ จุฬาลงกรณ์มหาวิทยาลัย
ปีการศึกษา 2563
ลิขสิทธิ์ของจุฬาลงกรณ์มหาวิทยาลัย

Thesis Title	Red Blood Cell Segmentation and Classification from Microscopic Images Using Machine Learning
By	Mr. Korranat Naruenatthanaset
Field of Study	Computer Engineering
Thesis Advisor	Associate Professor THANARAT CHALIDABHONGSE, Ph.D.
Thesis Co Advisor	Associate Professor DUANGDAO PALASUWAN, Ph.D.

Accepted by the FACULTY OF ENGINEERING, Chulalongkorn University in Partial Fulfillment of the Requirement for the Master of Engineering

-- Dean of the FACULTY OF ENGINEERING

(Professor SUPOT TEACHAVORASINSKUN, D.Eng.)

THESIS COMMITTEE

-- Chairman

(Assistant Professor SUEBSKUL PHIPHOBMONGKOL, Ph.D.)

-- Thesis Advisor

(Associate Professor THANARAT CHALIDABHONGSE, Ph.D.)

-- Thesis Co-Advisor

(Associate Professor DUANGDAO PALASUWAN, Ph.D.)

-- Examiner

(Sipat Triukose, Ph.D.)

-- External Examiner

(Supakorn Siddhichai, Ph.D.)

กรณัฏฐ์ นฤนาทธนาเสฏฐ์ : การตัดแยกและจำแนกเม็ดเลือดแดงจากภาพถ่ายจากกล้อง
จุลทรรศน์ด้วยวิธีการเรียนรู้ของเครื่อง. (Red Blood Cell Segmentation and
Classification from Microscopic Images Using Machine Learning) อ.ที่ปรึกษา
หลัก : รศ. ดร.ธนารัตน์ ชลิดาพงศ์, อ.ที่ปรึกษาร่วม : รศ. ดร.ดวงดาว ปาละสุวรรณ

การวิเคราะห์รูปร่างของเม็ดเลือดแดงมีความจำเป็นต่อการวินิจฉัยในหลายโรคที่เกิดจาก
ความผิดปกติของเม็ดเลือดแดง ขั้นตอนการตรวจสอบนี้ใช้เวลานานและต้องการความเชี่ยวชาญ
และประสบการณ์ ด้วยเทคโนโลยีคอมพิวเตอร์วิทัศน์และการประมวลผลภาพทางการแพทย์มี
ความก้าวหน้าจึงสามารถนำมาใช้เป็นเครื่องมือ เพื่อช่วยนักโลหิตวิทยาวิเคราะห์ภาพเม็ดเลือดแดง
จากกล้องจุลทรรศน์อย่างอัตโนมัติทำให้ใช้เวลาและค่าใช้จ่ายที่น้อยลง งานวิจัยนี้เสนอวิธีใหม่ใน
การตัดแยกและจำแนกเม็ดเลือดแดงจากภาพถ่ายจากกล้องจุลทรรศน์ ซึ่งขั้นตอนเริ่มจากการเก็บ
ข้อมูลด้วยแอปพลิเคชันที่ได้พัฒนาขึ้นเพื่อการเก็บข้อมูลเม็ดเลือดที่แม่นยำ การปรับสีภาพโดยใช้
ค่าเฉลี่ยของสีของพื้นหลังเพื่อให้โมเดลเรียนรู้ได้อย่างไม่อคติไปทางสี หลังจากนั้นเม็ดเลือดแดงที่
ซ้อนทับถูกตัดแยกด้วยวิธีใหม่โดยการหาจุดเว้าของเม็ดเลือดแดงและใช้วิธีการหาวงรีที่เหมาะสมใน
การประมาณรูปทรงของเม็ดเลือดแดง ในขั้นสุดท้ายคือการจำแนกเม็ดเลือดแดงออกเป็น 12 ชนิด
โดยใช้ EfficientNet-B1 อย่างไรก็ตามในการจำแนกออกเป็นหลายชนิดโดยใช้การเรียนรู้เชิงลึก
ปัญหาที่พบบ่อยคือความไม่สมดุลของข้อมูลเพราะตัวอย่างที่ปกติมักมีจำนวนมากกว่าตัวอย่างของ
โรคที่หายาก เทคนิคที่ช่วยในการแก้ปัญหาความไม่สมดุลถูกนำมาวิเคราะห์เพื่อลดในปัญหานี้ ผล
การทดลองแสดงให้เห็นว่าการใช้เทคนิคการปรับสมดุลของน้ำหนักร่วมกับเทคนิคการเพิ่มข้อมูล
จากข้อมูลเดิม สามารถช่วยแก้ปัญหาความไม่สมดุล

สาขาวิชา	วิศวกรรมคอมพิวเตอร์	ลายมือชื่อนิสิต ....
ปีการศึกษา	2563	ลายมือชื่อ อ.ที่ปรึกษาหลัก ....
		ลายมือชื่อ อ.ที่ปรึกษาร่วม ....

6170107821 : MAJOR COMPUTER ENGINEERING

KEYWORD: red blood cell segmentation, red blood cell classification, convolutional neural network (CNN)

Korranat Naruenatthanaset : Red Blood Cell Segmentation and Classification from Microscopic Images Using Machine Learning. Advisor: Assoc. Prof. THANARAT CHALIDABHONGSE, Ph.D. Co-advisor: Assoc. Prof. DUANGDAO PALASUWAN, Ph.D.

Red blood cell morphology analysis plays an essential role in diagnosing many diseases caused by RBC disorders. This manual inspection is a long process and requires practice and experience. Since recent computer vision and image processing in the medical imaging area can provide efficient tools, it can help hematologists to automatically analyze images from a microscope in a reduced time and cost. This research presents a new method to segment and classify RBCs from blood smear images. The process started from data collection, which a new application was created for precisely labeling. The normalization was done to reduce the color space and allowed the trained model to not be biased on color. Then, overlapping cells were separated using a new method to find concave points and use direct ellipse fitting to estimate the shape of a single RBC. Lastly, classification using EfficientNet-B1 on 12 red blood cell classes was done. However, to classify multiple classes with deep learning, imbalance problems are common in medical imaging because number of normal samples is always higher than number of rare disease samples. The imbalanced handling techniques were analyzed to deal with this problem. Experimental results showed that the weight balancing technique with augmentation had the potential to deal with imbalance problems.

Field of Study:	Computer Engineering	Student's Signature ....
Academic Year:	2020	Advisor's Signature ....
		Co-advisor's Signature ....

ACKNOWLEDGEMENTS

This project would not have been possible without the support of many people. I would like to thank my supervisors, Prof. Thanarat Chalidaphongse and Prof. Duangdao Palasuwan for their patience, guidance, kindness, and for being great teachers. I have received much invaluable feedback for my work and my life. Thanks to Prof. Nantheera Anantrasirichai for assistance, excellent encouragement, and guidance. Further, thanks to the member of PIC Lab for suggestions throughout this project.

I am grateful for my parents whose constant love and support keep me motivated and confident.

Korranat Naruenatthanaset

TABLE OF CONTENTS

จุฬาลงกรณ์มหาวิทยาลัย
CHULALONGKORN UNIVERSITY

1. Introduction

In a hospital, red blood cell (RBC) morphology analysis is a subprocess in the Complete Blood Count (CBC) process. This analysis plays an essential role in diagnosing many diseases, caused by RBC disorders, such as anemia, thalassemia, sickle cell disease, etc. The analysis mainly focuses on the shape, size, color, inclusions, and arrangement of RBCs (Ford, 2013). Generally, the normal RBC shape is round, biconcave, with a pale central pallor and of 6–8 μm diameter. A hematologist manually analyzes the blood cells under a light microscope from blood smear slides. This manual inspection is a long process and also requires practice and experience. Since recent computer vision and image processing in the medical imaging area can provide efficient tools, it can help hematologists to automatically and less subjectively analyze RBC images from a microscope in a reduced time and cost.

For the student training process in the Faculty of Allied Health Sciences at Chulalongkorn university, to expert in RBC morphology, students need to practice with microscopes and be guided by staff and professors that take a lot of time to thorough care of every student. The students must take a picture of the RBC slide through the microscope lens and learn how to classify RBCs by themself that can lead to misunderstanding. Automating RBC counting and classifying would help to guide the students so they can learn by themselves which also reduces the workload for professors and staff.

Figure 1-1 Students manually take a photo of the blood smear slides using a smartphone to do the laboratory test by themself.

Most of the previous RBC imaging research works were to classify RBCs to identify the type of RBCs in the images. Normally, the image, captured from a microscope, contains many cells so the cell segmentation must be done before proceeding to the cell classification process. The previous works have employed typically image processing techniques to the recent state-of-the-art deep learning techniques which have improved accuracy significantly. However, there are still several challenges to achieve this goal. Since RBCs in the image may overlap with each other, it is hard to find the edge of the cell. In the manual process, the hematologist usually avoids selecting an area that has a lot of overlapping cells. But in some situations, especially in automated methods, it is difficult to avoid these areas because the cells stick together leading to incorrect predicted results. Thus, automated segmentation must be able to handle the overlapping cells so that it can cover the real situation. In addition, blood smear slides may not have the same environment, such as lighting, zoom scale, and camera.
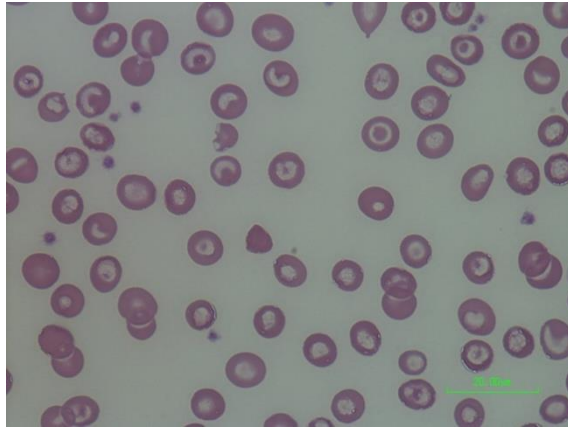
*Figure 1-2 Sample of RBC image from a microscope.*

Recently, a deep convolutional neural network for object detection and semantic segmentation has begun to be used for RBC detection (Qiu et al., 2019; Shakarami, Menhaj, Mahdavi-Hormat, & Tarrah, 2021; Wong et al., 2021). The benefits of these deep end-to-end methods are that, first, they allow training a possibly complex learning system represented by a single model, bypassing the intermediate layers usually found in the traditional pipeline approach. Secondly, it is possible to design a model that performs well without deep knowledge about each sub-problem in the complex system. However, the end-to-end approach is an infeasible option in some cases, for example, a huge amount of data is not available, the intermediate results are needed, as well as the computational resources are limited.

For this research, our goal is to develop the RBC segmentation and classification that require low computational complexity resources such as mobile phones and tablets so that mobile application can run in reasonable time for the hematologist training. Secondly, the application requires to have an interface that shows individual cell colored based on its type, for a real-time user interaction feature. By using end-to-end deep learning object detection or instance segmentation would not be feasible to serve this purpose well comparing to the

very efficient and accurate traditional low-level computer vision approach we proposed in this research.

Although deep learning has shown remarkable results in computer vision, these approaches still need lots of data to achieve a good outcome. Nevertheless, RBC datasets are difficult to collect because some RBC types can only be found in specific diseases, and these may only be found in specific geographic regions. Accordingly, each dataset usually has an imbalance problem. Moreover, even then different specialists might give different results, depending on their expertise, and so shifts the analytical balance towards being subjective.

This research presents a new framework for RBC data collection, RBC segmentation using ellipse fitting, and classification via the use of EfficientNet (Tan & Le, 2020). The main contributions of this thesis are: (i) an application for helping labelers to label the ground truth in blood smear images, (ii) a new method to separate the overlapping cells based on the concave points of the border of RBCs, and (iii) RBC classification with analysis of imbalanced datasets using data augmentation, weight normalization, upsampling, and focal loss (Lin, Goyal, Girshick, He, & Dollár, 2018) on multi-class classification.
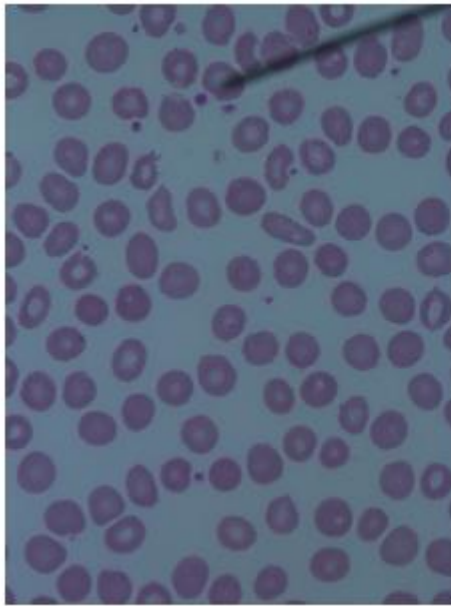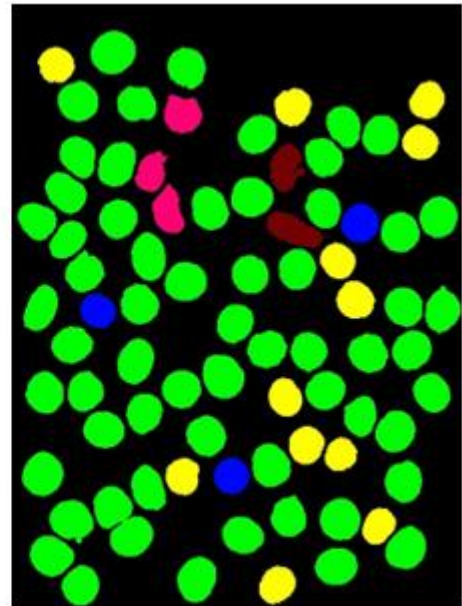
Figure 1-3 (a) Input image, (b) Expected output image

1.1. Aims and Objectives

The objective of this study is to develop a method for red blood cell segmentation and classification from microscopic images.

1.2. Scope of study

- The images that were used to train and test in this study were collected and labeled by specialists from the Faculty of Allied Health Sciences, Chulalongkorn University.
- This study focuses on RBCs in the image that do not rip by borders of the image and RBCs are not overlapped by other objects such as scale bar and pointer from microscope software.

2. Literature Survey

In this chapter, previous studies that are related to this study are reviewed. We organize the chapter into three sections. The first section summarizes recent related works in the literature in order of published year. The next two sections review techniques used in RBC segmentation and classification respectively. The conclusion of each topic technique is then described at the end of this chapter.

2.1. Previous studies

(Ritter & Cooper, 2007) proposed RBC segmentation on blood smear slides of canine blood using graph algorithm-based to find the edge of the RBCs. The algorithm firstly threshold the greyscale images. Then, connected components were found by Dijkstra's shortest path algorithm. 47 images were tested with both normal and diseased RBCs with 97.3% accuracy and 51 images also were tested with 99.0% accuracy. The proposed method is faster than prior works. The results work well for single cells and torching cells. It cannot handle or separate overlapping cells.

(Khashman, 2008) presented blood cell classification which classifies into 3 major blood types, RBC, white blood cell (WBC), and platelet. The classifier is an artificial neural network (ANN) with 196 neurons for input, 40 neurons for one hidden layer, and 3 neurons for output. Global pattern averaging, by dividing the image into 196 blocks then the pixels in the block were average, was used to extract features from a single cell image as the input for ANN. 99.17% accuracy was achieved with 60 training images and 300 testing images.

(Soltanzadeh & Rabbani, 2010) presented 3 types of RBC classification, ovalocytes, dacrocytes, and burr cells using average and variance distance from mass center to edges of the cell. The results were tested with 100 single cell images from each RBC type that shows a low error rate in all 3 types. This work used only 2

statistic values to classify 3 types. To classify more classes, this method needs more features to improve predict more types of RBC.

(Kareem, Morling, & Kale, 2011) proposed a counting method without preprocessing. First, the image was converted to grayscale. Next, dilation was used to remove small objects such as platelets or noises, using a ring shape kernel with 70% of RBC size. According to the image without preprocessing, the background pixels had higher values than object pixels, so dilation made objects smaller or disappearing. Then, erosion using a disk shape kernel recovers the cell from the previous step. The image was converted into a ratio transformed image in which the center of RBC has high intensity by average values of pixels in the ring shape kernel to disk shape kernel inside the ring. Finally, the result was achieved by counting the peak intensities. This method seems to be suitable for RBC with a circular shape because it used a circle base for dilation, erosion, and finding the ratio. However, there can miss detecting RBC that is not a circular shape such as sickle cell, ovalocyte, etc.

(Habibzadeh, Krzyzak, Fevens, & Sadr, 2011) segment using Watershed algorithm on grayscale and classify RBC and WBC using the size of RBCs. This work also did de-noising with Bivariate wavelet and edge-preserving with Kuwahara filter. Better counting result was shown compared with the Otsu threshold and Canny edge algorithm in 10 blood smear images. They were claimed better performance and lower complexity than previous works but did not show accuracy results.

(Cai, Wu, Zhang, Fan, & Ruan, 2012) proposed an RBC segmentation using an active appearance model (AMM) which can extract the cells from the background precisely. The output was shown that it can use for counting and measurement of the cell. The AMM was built from training images and landmarks which work quite well in the study because of the circular shape of RBC. Though the work does not

provide statistical results, only showed output sample images. For other RBC types, the single AMM cannot totally match all RBC types.

(Rakshit & Bhowmik, 2013) presented a detection of sickle cell anemia. Sobel edge detection was used on grayscale, and only one manual roundness feature was used to classify 2 classes: normal cells and sickle cells. The accuracy is 95.8% on 5 samples which is quite lower than other works.

(Mazalan, Mahmood, & Razak, 2013) used the circular Hough transform (CHT) to count RBCs from blood smear images. This algorithm is a circle finding which is work best on circular shape object with a known radius, so it is work best for Normal cells. This work has achieved 91.87% accuracy from 10 sample images. The miss-detected cells were overlapping cells and non-circular RBC.

(Tomari, Zakaria, Jamil, Nor, & Fuad, 2014) proposed RBC detector and classifier. First, they used the Otsu threshold on a green channel of a blood smear image to extract RBC regions from the background. They perform three steps for post-processing to remove other objects, morphological operation (erosion and dilation), connected component labeling, and bounding box filter. Besides, the overlapping cells were identified by finding large regions. After that, features were calculated from RBCs to train a neural network. There were two main features, compactness, and moment invariant (seven Hu moments). The neural network was trained on 100 images and tested on 50 images to classify into two types, normal and abnormal. The accuracy, precision, and recall were 83%, 82%, and 76% respectively. They ignored the overlapping cells by selecting the cells that have a size approximate to a normal cell, then classified only single cells. The neural network had only one hidden layer. According to the number of features and the number of layers in this model, it might need more features and layers to increase accuracy or classify more types.

(Lee & Chen, 2014) proposed the hybrid neural network architecture for RBC classification. First, the overlapping cells were segmented and separated by finding edges inside the cells. The top cell was extracted by considering the smoothness of endpoints between the edge. After that, RBCs were extracted by applying a closed region mask based on edge.   Then, the features were generated from RBCs for feeding into the neural network. The features were divided into two groups, shape feature, and texture feature. Both features were used in the hybrid neural network. The difference between a neural network and this network is this network predicts the cells that are normal or abnormal cells by shape features with higher priority than texture features. Finally, both features had the same priority to classify four types if the cell was abnormal. In this study, overlapping segmentation was described, but it was not evaluated. The result of classification into five types is better than the neural network with the same number of layers which is 88.25% accuracy on 200 single-cell images. This architecture seems to make sense with a human visual concept.   The method used a small neural network and manual feature extraction.   Therefore, it might not be sufficient to classify more types according to the number of layers.

(Chandrasiri & Samarasinghe, 2014) used Otsu thresholding to segment RBC and used rule-based with 4 features to classify 5 types of RBCs. To separate overlapping cells, extended-minima transform is used to find markers and separate touching cells, then, Euclidean distance transform following by Watershed transformation. The segmentation accuracy on 10 images is 99.68% which is better than only distance transform, marker controlled, and Blob detection. In the classification step, 4 features were created to classify Normal cells, Macrocyte, Spherocyte, and Microcyte. The features involve length, diameter, area, the ratio between cell area and central pallor. The accuracy of 4 abnormal types is in the range of 91% - 97% but the Normal cell is not evaluated. In this study, the features

are created to only classify these RBC types which make sense for the shape of the selected RBC types. It might classify more types if it does not have more features.

(González-Hidalgo, Guerrero-Peña, Herold-García, Jaume-i-Capó, & Marrero-Fernández, 2015) proposed a method to separate overlapping cell clusters using concave points. First, RBC contours were extracted from a background image using an edge finding. The k-curvature technique was used to find the concave points by considering a slope of the interesting point. After that, the curve between concave points was used to estimate an ellipse by the ellipse fitting method with the proposed constraints. This study was tested on three different types of images, generated ellipse cluster images, real RBC images, and synthetic images. The synthetic images were generated by single-cell combining. The result seems good for all tested images, and the accuracy was 100% on synthetic samples and 96.52% on real images with 2– and 3-object clusters. However, the undetected objects occurred due to non-detect of concave points or highly overlapping.

(Nugroho, Akbar, & Murhandarwati, 2015) proposed a method to detect malaria cells. First, the blood smear image was converted from RGB to HSV color space, then selecting the S channel because of the quality of contrast. Next, to enhance the images, the contrast stretching method is followed by a median filter for denoising. In the segmentation process, the K-means algorithm was used to separate the cells of background, however, the study does not show how to select the K parameter or evaluate the performance. To classify 3 types of malaria, a neural network with 1 hidden layer was used. 6 features were calculated as an input. The overall accuracy is 87.8 on 60 images. It used K-cross validation to evaluate the performance, but it does not tell how to separate the dataset.

(Sharma, Rathore, & Vyas, 2016) proposed a method to detect sickle cell anemia and thalassemia. First, the blood smear image was pre-processed by the median filter. Next, the marker-controlled watershed was used for segmentation.

Finally, the k-nearest neighbor was used to classify the cells into four types using metric value, aspect ratio, and radial signature between radial distance and polar coordinate. The accuracy was 80.6%. In this study, the classifier was trained and tested using 100 images. It might overfit the result because there are only a few images. For segmentation, it used manual points to make seed points before applying the watershed method. It takes time for pointing to the entire image.

(Romero-Rondón, Sanabria-Rosas, Bautista-Rozo, & Mendoza, 2016) proposed a method to detect overlapping cells that was based on K-means clustering. The first step is a preprocess which removes WBCs and platelets by applying subtraction between the image and morphologic operation on the S channel in HSV. To separated overlapping cell contour, the number of cells in contour determines by cell area distribution between 1 – 3 cells. For more than 3 cells in a cluster, the Hough circle transform was used for the trade-off between the number of cells defined by area. After that, to find the marker for using Watershed, 3 approaches were used: erosion, Hough, and K-means respectively. The last step after applying Watershed, Bézier was used to estimate the missing edge. The sensitivity is 98.37% tested on 50 images. The study shows error images that occurring on the wrong marker number.

(Ahmad, Abdullah, & Sabudin, 2016) compared 3 overlapping cell algorithms: Iterative randomized irregular circle detection (IRIC), Circle Hough transform (CHT), and Edge drawing circle (EDCircle). IRIC shows the best result while the lowest is EDCircle on 2 – 5 overlapping cells.

(Liang et al., 2016) detected malaria cells using a convolutional neural network (CNN). The network has 6 convolutional layers, 2 pooling, and 3 connected layers. The output is sigmoid for binary classification: uninfected and infected cells. This dataset has 27,578 single RBC images with a 1:1 ratio for both classes. 97.37% accuracy was achieved with 90% training and 10% testing sample on 10-fold cross-

validations. The study also shows better performance compared with the transfer learning model which is the AlexNet model pre-trained on the CIFAR-100 dataset.

(Tyas, Ratnaningsih, Harjoko, & Hartati, 2017) compared the results between ANN and CNN. The ANN has 43 inputs computed from Invariant moments, GLCM (Grey Level Co-occurrence Matrix), and color features. It has 1 hidden layer with 10 maximum neurons in experiments. CNN is based on the LeNet-5 model. The CNN input images are 32*32 pixels. However, the accuracy on ANN is better than CNN, 93.22% and 92.55% respectively. The dataset consists of 256 single-cell images. In this study, the dataset quite has a small number of samples. The CNN model needs more samples for training to achieve high accuracy.

(Xu et al., 2017) proposed a method to segment touching cells, and classify RBC using the convolutional neural network (CNN) into 8 types. First, to segment the RBCs, the entropy of grayscale level was computed within overlapping sliding windows, then, high entropy was extracted as an ROI mask image. They separated touching cell contours using a distance transform to find seed points for each cell. Then, the seed points were used for the segmentation of the cell by the random walk method. As a result, it could separate touching cells but not for overlapping cells. Lastly, the image was normalized and fed into CNN with ten layers to classify into eight types. The mean accuracy of 5-fold cross-validation is 87.50% on 7224 single cells.

(Acharya & Kumar, 2017) presented a method to classify 11 types of RBC disorders. First, WBCs were identified by the minimum intensity of the L layer in LAB color space, and platelets also were removed by erosion operation with a disk shape element. The blood smear images were segmented by Otsu's thresholding. To separate overlapping cells, the modified distance transform was applied and the "regionprops" function was used for recovering the cell area. For classification, ruled based operation was used to classify 11 types using 8 features. The features are

mostly based on geometric shapes. The accuracy was 98% on over 1000 single cells with 8 blood smear images. However, the data is imbalanced, mostly normal cells, macrocytes, and spherocytes, with only a few sickle cells, hypochromia, and elongated cells. The difference in this study is the types that were selected are concerned with central pallor based on the focused diseases, such as normocyte and normocyte with central pallor, etc.

(Zhang, Li, Xu, & Li, 2017) used deformable U-net to segment and classify a sickle cell (normal cell and sickle cell). U-net is a fully CNN that is popular in medical computer vision research for the semantic segmentation problem. Also, it can classify the image at a pixel level. The architecture of U-net can be divided into 2 parts, encoder, and decoder. The encoder performs convolution operation following by max-pooling to down-sampling the data which reduces the resolutions but increases depths. The decoder performs a deconvolution operation to up-sampling the data which increases resolution but reduces depts back to the same as the input. Though, the deformable convolution was used instead of normal convolution which can help the U-net model robust for translation and rotation. This technique is better than augmentation on training times. The dataset has 128 samples, 88 for training and 40 for testing. The result of this network is better than the baseline U-net model, 82.7% over 73.1% for classification and 97.8% over 94.7% for only segmentation. However, this model also used four times longer of training than U-net. In this study, in a single RBC, the model can predict 2 types because it classifies every pixel.

(Durant, Olson, Schulz, & Torres, 2017) proposed a very deep CNN for classifying ten types of RBC (including overlapping cells). This network had more than 150 layers with dense shortcut connections, called DenseNet (Huang, Liu, van der Maaten, & Weinberger, 2018). The shortcut connection helps CNN avoiding a vanishing gradient problem on the very deep networks. Accordingly, the problem occurs when CNN has a lot of layers; the gradient will be led to zero after applying

many non-linear functions. The dataset has 4032 labeled cell images which is divided into 2989 training data and 748 testing data. The result was shown with 90.60% overall accuracy. However, the dataset is highly imbalanced. Further evaluation was done that on low sampling class had low F1-score, precision, and recall.

(Gopakumar, Swetha, Siva, & Subrahmanyam, 2018) presented automated slide scanner to detect malaria cells using CNN. The proposed method started with Otsu's thresholding ROI out of the background. To separate overlapping cells, the distance transform was used to locate the RBCs as markers, and Watershed was used to segment the cell area from the markers. For classification, 4 manual designed CNN was used to classify non-infected and infected cells. The low CNN layer was designed for low-performance edge computing. The evaluation was compared with SVM with 14 feature inputs: 4 texture, 4 statistics, 2 computed gradients, and 4 computed subregions constituting. The CNN outperforms SVM by 98.81% and 96.38% sensitivity on 11,200 training images.

(Alom, Yakopcic, Taha, & Asari, 2018) used Inception recurrent residual convolutional neural network (IRRCNN) to classify WBC and RBC. The model is a hybrid deep CNN based on inception, residual networks, and recurrent neural network. For RBC classification, the model classified 10 RBC classes which is a dataset of (Durant et al., 2017). The accuracy is 99.94% that outperformed all previous studies.

(Sadafi, Radolko, Serafeimidis, & Hadlak, 2018) used Fully-AlexNet deep learning model to segment RBCs from blood smear images. The model was converted from AlexNet (Krizhevsky, Sutskever, & Hinton, 2012) which is for classification by (Long, Shelhamer, & Darrell, 2015). The images were divided into multiple tiles that have overlapping parts, then, fed into the network. The accuracy is 93.12% on 52 blood smear images which 10% is for validation. However, the limitation of the segmentation method for RBCs is the overlapping cells. In this study,

it did not have post-processing to separate the overlapping cells but, from observation on sample ground truth images, the labels were done by keeping a space between the cells that closed to each other. For this cause, the results seem to not have a perfect shape, but it can identify the location of RBCs.

(Aliyu, Razak, & Sudirman, 2019) compared RBC segmentation techniques for sickle cells. The segmentation techniques are Watershed, edge detection, Laplacian of Gaussian, and Otsu thresholding. The result was shown that the Otsu thresholding had the highest accuracy, sensitivity, and specificity among the rest on 30 blood smear images.

(Qiu et al., 2019) proposed multi-label RBC detection which is an object detection problem using Faster R-CNN (Ren, He, Girshick, & Sun, 2016). Faster R-CNN is an object detection based on a region proposal network. For this study, Resnet-101 (He, Zhang, Ren, & Sun, 2015) was used as a backbone of the classification model. Normally, other studies used multi-class problems, 1 object for 1 class. In a multi-label task, 1 object can have multiple classes. The evaluation was done with 313 blood smear images with 0.899 average precision (AP). Further analysis also was done on multi-label classification using Resnet-50. The best accuracy is 0.932. However, the Faster R-CNN identified overlapping cells as 1 connected component. Watershed seems to separate the overlapping cells better. Moreover, U-net, which is FCNN, was discussed that it can segment the precise shape of RBCs but still cannot separate overlapping cells.

(Pasupa, Vatathanavaro, & Tungjitnob, 2020) used a focal loss (Lin et al., 2018) for 3 class canine RBC classification which helped to improve the performance on the imbalance dataset. First, the blood smear images were segmented based on the Hough circle transform. Next, for classification, ResNet-50 and DenseNet-121 were evaluated the performance with normal cross-entropy loss and the focal loss. The result was shown that DenseNet-121 with the focal loss performs the best accuracy

and f1-score, 95.60% and 92% respectively. The dataset has 22 dog blood smear images contained 3392 single cells, which divided into 70% training data and 30% training data. Moreover, Over-sampling and under-sampling techniques also were evaluated. It was shown that the over-sampling had slightly lower performance than the focal loss.

(Batitis et al., 2020) used a decision tree to classify 10 types of RBCs. The process started with finding contours using Canny edge detection on grayscale. For classification, 6 features were calculated for the input of the decision tree. The decision tree has 9 nodes for classifying 10 RBC types. The evaluation was done on 40 blood smear images that have 600 labeled single cells. The average accuracy is 89.31%. The computed reliability of each node in the decision tree was also shown. The lowest performance is on Target cells and Stomatocytes because the difference in both types is on central pallor which difficult to segment the precise shape. However, the dataset is highly imbalanced, the minimum is only 3 cells, but the maximum is 173 cells.

(Parab & Mehendale, 2020) used the CNN to classify 10 types of RBC. The pre-processing was used Canny edge detection on grayscale for extracting the edge of RBCs. For classification, the CNN model had only 2 convolution layers. The performance was tested on a validation set which has 5000 images, 500 for each type. The accuracy is 98.5. However, the study was described the training dataset, validation dataset, and testing dataset, but it does not specify the number of RBCs, only in the validation dataset.

(Abdulkarim, Razak, Sudirman, & Ramli, 2020) used AlexNet model to classify 15 RBC types. First, the individual RBC was extracted from blood smear images by Otsu thresholding. The dataset has over 9,000 single RBC images which each type has 750 cells from 130 patients. The accuracy is 95.92%. In this work, the abnormal types

contained a cluster of RBCs which is different from other works that focus on only single cell types.

(Alzubaidi, Fadhel, Al-Shamma, Zhang, & Duan, 2020) proposed 3 type RBC classification using CNN including normal, sickle cells, and others. Three CNN models were designed and compared the performance. The best model has 23 layers and it was trained on 3 different datasets including the dataset from (González-Hidalgo et al., 2015). The model achieved 99.54% accuracy and 99.98% accuracy on the model plus a multiclass SVM classifier. The model also used transfer learning and several augmentation techniques to overcome the small dataset for training.

(de Haan et al., 2020) proposed an automated screening for sickle cells using semantic segmentation. The proposed method has 2 U-net models. The first model is for enhancing the blood smear images. The second model is for segmentation into 2 types which are normal and sickle cells. For the results, the method was evaluated on 96 patients including 9,630 RBCs and achieved ~98% accuracy.

(Delgado-Ortet, Molina-Borrás, Alférez, Rodellar, & Merino, 2020) used fully convolutional neural networks to segment RBCs from blood smear images and CNN to classify malaria. The segmentation model has 7 layers including down-sampling and up-sampling layers. The classification model has 13 layers. Both models are self-designed. The evaluation was done on 331 images dataset with 98.72% and 75.39% accuracies on segmentation and classification, respectively.

(Rahman et al., 2021) proposed 15 type RBC classification using a rule-based method on color, morphology variation, and central pallor of RBCs. First, the blood smear image was preprocessing and segmented WBCs, RBCs, and platelets by XOR operation between a binary image and a cell mask. After that, each feature was extracted by image processing. Then, the rule-based condition was used to classify into each RBC type. The performance was tested on 250 blood smear images. The average accuracy was 97%.

(Shakarami et al., 2021) used YOLOv3 to detect RBCs, WBCs, and platelets. EfficientNet was used as the backbone of the YOLOv3. The dataset in this work has 364 images with 3,943 cells and 945 cells for training and testing. The activation function also was modified to the Swish activation function instead of LeakyReLU. The average precisions are 90.25%, 80.41%, and 98.92% for platelets, RBCs, and WBCs respectively.

(Wong et al., 2021) proposed RBC classification with 3 methods. Our dataset also was used in this work. First, to segment RBCs from blood smear images, Otsu thresholding was used and then SVM for dividing a single cell and overlapping cells. SVM and TabNet were used as a classifier for 11 RBC types with 78.2% and 73.0% average F2-scores for SVM and TabNet respectively. To overcome the imbalance problem, SMOTE with cost-sensitive learning was used while training. Lastly, U-net was used to classify 6 RBC types which achieved a 78.2% F2-score.

From our survey, most of blood smear imaging research works can be divided into 3 groups (Hegde, Prasad, Hebbar, & Sandhya, 2018) based on subtypes of blood cells: RBCs, WBC, and platelets. Most of the works have a common objective which is to help hematologists who must count and analyze RBCs manually to detect diseases. The number of research apparently correspond to the degree of the disease. WBCs studies mostly focus on leukemia. RBCs studies focus on malaria, sickle cell disease, and other abnormalities. Platelet studies are only counting and classification on normal and abnormal.

In the next sections, previous works on RBCs segmentation and RBCs classification, which are the area that this thesis focuses on, are reviewed.

2.2. RBC Segmentation

The objective of RBC segmentation is to extract RBCs from blood smear images. The images are usually captured from a microscope at several magnification levels. The scale suitable to observed RBC is 400x to 1000x. The 400x magnification level can see an area with 0.45mm, or 450 microns (μm) diameters while the 1000x can see an area with 180 μm diameters. The RBCs normally have a diameter around 6 – 13 μm. Although, the RBC shape is a biconcave disk, in the microscope, it looks like a donut, circular shape with a white area in the middle as central pallor. The color of the cells is red to slightly purple which is much high contrast compared to the background which has lower contrast.

Table 2-1 summarizes the segmentation and overlapping cell separation methods used in the previous research. The methods can be divided into 2 groups: traditional image processing, and deep learning methods.

For traditional image processing methods, the first step of segmentation usually was converting the color blood smear images to grayscale. Then, image normalization, blurring, and thresholding were performed to enhance the segmentation. To extract the precise shape of RBCs, several methods had been proposed such as thresholding, edge detection, and circular shape detection algorithms. After that, the overlapping cell separation was performed to separate single cell from a group of the RBC contour. The characteristics of clusters of RBCs are used to detect and split each cell such as the circular shape of individual RBC or concave point of overlapping cells. Then, morphology operation was done for extracting RBC contours.

Recently, the deep learning approaches have been used for RBC segmentation. The most model used in many works was a fully convolutional neural network where input is the blood smear image, and the output is also an image that

each pixel is predicted to be either RBC pixel or a background pixel. However, the limitation of this method is that it cannot separate a cluster of RBCs or it needs post-processing for this task. Moreover, creating a dataset for training requires a manual label process for all the pixels which is very labor-intensive task.

Table 2-1 Summary of RBC segmentation methods and overlapping separation methods of previous research

Author	Segmentation Method	Overlapping Separation Method
(Ritter & Cooper, 2007)	Dijkstra's shortest path on RBC border	-
(Soltanzadeh & Rabbani, 2010)	Otsu thresholding	-
(Habibzadeh et al., 2011)	Otsu thresholding	Watershed
(Kareem et al., 2011)	Ring dilation and erosion	-
(Cai et al., 2012)	Active appearance model (AAM)	-
(Rakshit & Bhowmik, 2013)	Sobel edge detection	-
(Mazalan et al., 2013)	Circle Hough transform	-
(Lee & Chen, 2014)	Otsu thresholding	Canny edge inside contour
(Tomari et al., 2014)	Otsu thresholding	-
(Chandrasiri & Samarasinghe, 2014)	Otsu thresholding	Extended-minima transform, Euclidean distance transform, Watershed
(Nugroho et al., 2015)	K-means with marker based on distance	-
(González-Hidalgo et al.,	-	K-curvature for

Author	Segmentation Method	Overlapping Separation Method
2015)		concave point then ellipse fitting
(Sharma et al., 2016)	Marker-controlled Watershed	-
(Ahmad et al., 2016)	Otsu thresholding	IRIC, Circle Hough transform, EDCircle
(Romero-Rondón et al., 2016)	Otsu thresholding	erosion, Hough, K-means
(Tyas et al., 2017)	Histogram equalization	
(Xu et al., 2017)	The entropy of grayscale level on sliding windows	Distance transform, then random walk method
(Acharya & Kumar, 2017)	Otsu thresholding	Distance transform
(Gopakumar et al., 2018)	Otsu thresholding	Distance transform, then Watershed
(Sadafi et al., 2018)	FCN-AlexNet	-
(Aliyu et al., 2019)	Otsu thresholding	-
(Pasupa et al., 2020)	Circle Hough transform	-
(Batitis et al., 2020)	Canny edge detection	-
(Parab & Mehendale, 2020)	Canny edge detection	-
(Abdulkarim et al., 2020)	Otsu thresholding	-
(Delgado-Ortet et al., 2020)	Fully convolutional neural network	-
(Rahman et al., 2021)	XOR with mask	-
(Wong et al., 2021)	Otsu thresholding	-

2.3. RBC Classification

Hematologists can use RBC classification to automate a complete blood count (CBC) process leading to time and cost saving. The automatic classifier can also help detecting various diseases associated with RBC abnormalities, such as Malaria and Thalassemia. The works in this discipline can be split into three categories based on their intended use.

1. Blood cell classification which classifies into RBCs, WBCs, and platelets.
2. Multi-type RBC classification which classifies into multi types.
3. Specific disease classifications such as Malaria, Thalassemia, Sickle cell disease.

Table 2-2 summarizes the methods, datasets, RBC types, and results of previous works on RBC classification. Almost every research was evaluated using their-own dataset yielding nearly perfect results. Moreover, each research also focuses on a different set of RBC types. Thus, it is hard to compare each method in a straightforward way. Below we review the research works on RBC classification grouping by approach into 2 groups: traditional image processing techniques and modern deep learning approaches.

1. **Image processing approaches**

In this approach, the RBCs are classified based on manual features that were observed on RBC appearance such as size, roundness, color, etc. After that, the features are used to classify on condition probability algorithms such as rule-based and decision tree. The limitation of this method is varieties of environments. It might not tolerate different environments. To add multiple classes, the complex rule-based method increases the difficulty of the research.

2. Deep learning approaches

RBC classification using deep learning was started to use on a neural network. The manual feature extraction was still used in this step. After that, CNN was used since AlexNet outperformed on ImageNet competition. The CNN model can be trained without manual feature extraction. The classification model on general tasks can also be used with high performance on other tasks including RBC classification. To develop the RBC CNN classification model, the model architecture and RBC dataset are the most important parts instead of fully designing all the steps likes the previous method. For this reason, the model can classify multiple types with ease only provide RBC images.

In the recent research, semantic segmentation and object detection was used to detect and classify RBC which is an end-to-end deep learning. For semantic segmentation, the model can segment and classify the whole blood smear image at pixel level, but it was difficult to create a dataset for this task. Moreover, the research nowadays still has only a small dataset. For object detection, the outputs are the type of RBCs and bounding box. The dataset for object detection is easier than semantic segmentation.

To train the RBC classification, the data imbalance is a problem that is difficult to avoid when adding multiple RBC types because some rare types, which are difficult to find, always have less than normal RBC. This problem also is a common problem in a medical classification task. To handle the imbalance problem, several techniques can be added to the training step. Augmentation is a must step to generalize the model, but it can use to perform upsampling and downsampling to handle the imbalanced dataset. In the training step, weight balancing is used when backpropagation. Adjusting the loss function also can help the model not bias to the main class.

Table 2-2 Summary of RBC classification method, dataset, RBC type, and result of previous research

Author	Classification Method	Dataset (training, testing)	RBC Types	Result (Accuracy)
(Khashman, 2008)	Neural Network	60 cells training set, 300 cells test set	Platelet, RBC, WBC	99%
(Soltanzadeh & Rabbani, 2010)	Average and variance features	100 cells	Burr cell, Discocyte, Ovalocyte	96.9%
(Habibzadeh et al., 2011)	Area size	10 blood smear images	RBC, WBC	-
(Rakshit & Bhowmik, 2013)	roundness feature	5 blood smear images	Normal, Sickle Cell	95.80%
(Lee & Chen, 2014)	Hybrid neural network	400 single cells images (200, 200)	Burr cell, Horn Cell, Normal, Ovalocyte, Sickle Cell	88,25%
(Tomari et al., 2014)	Neural network	150 single cells images (100, 50)	Abnormal, Normal	83%
(Chandrasiri & Samarasinghe, 2014)	4 features decision	-	Macrocyte, Microcyte, Normal,	91-97% on each

Author	Classification Method	Dataset (training, testing)	RBC Types	Result (Accuracy)
	tree		Ovalocyte, Spherocyte	abnormal type
(Nugroho et al., 2015)	Neural network	60 single cells images	Normal, Malaria	87.8%
(Sharma et al., 2016)	KNN	100 blood smear images	Normal, Ovalocyte, Sickle Cell, Teardrop	80.60%
(Liang et al., 2016)	CNN	27578 single cell images (90%, 10%)	Malaria	97.37%
(Durant et al., 2017)	DenseNet151	4032 single cells (2989, 748)	Acanthocyte, Burr cell, Normal, Ovalocyte, Overlapping cells, Schistocyte, Spherocyte, Stomatocyte, Target Cell, Teardrop	90.60%
(Zhang et al., 2017)	Deformable U-net	128 blood smear images (88, 40)	Normal, Sickle Cell	82.7%
(Tyas et al., 2017)	ANN, CNN	256 single images	Acanthocyte, Normal, Cigar Cell,	93.22%, 92.55%

Author	Classification Method	Dataset (training, testing)	RBC Types	Result (Accuracy)
			Target Cell, Teardrop	
(Xu et al., 2017)	10 layers CNN	7224 single cells images (80%, 20%)	Burr cell, Dacrocyte, Elongated, Granular, Ovalocyte, Reticulocyte, Sickle Cell, Stomatocyte	87.50%
(Acharya & Kumar, 2017)	A decision tree with 11 features	8 blood smear images	Elongated, Hypochromic, Hypochromic macrocyte, Hypochromic microcyte, Macrocyte, Macrocyte without central pallor, Microcyte, Normal, Normal without central pallor, Sickle Cell, Spherocyte	98%
(Gopakumar et al., 2018)	4 layers CNN	11200 single cells images (90%, 10%)	Malaria	98.81 sensitivity

Author	Classification Method	Dataset (training, testing)	RBC Types	Result (Accuracy)
(Alom et al., 2018)	IRCNN	4032 single cells images (2989, 748)	Acanthocyte, Burr cell, Normal, Ovalocyte, Overlapping cells, Schistocyte, Spherocyte, Stomatocyte, Target Cell, Teardrop Cell	99.94%
(Qiu et al., 2019)	ResNet-50, Faster-RCNN	313 blood smear images	Burr cell, Elongated+Sickle, Granular, Normal, Reticulocyte, Stomatocyte	Detection AP 0.899, Classification 93.2%
(Pasupa et al., 2020)	DenseNet-121 Focal loss	22 blood smear images with 3392 single cells (70%, 30%)	Hypochromic, Normal, Target Cell	95.6%
(Batitis et al., 2020)	A decision tree	40 blood smear	Acanthocyte, Burr cell, Degmacyte,	89.31%

Author	Classification Method	Dataset (training, testing)	RBC Types	Result (Accuracy)
	with 6 features	images with 600 singles cells	Elliptocyte, Ovalocyte, Sickle Cell, Spherocyte, Stomatocyte, Target Cell, Teardrop	
(Parab & Mehendale, 2020)	2 layers CNN	5000 validation single cells images	Howell Jolly, Macrocyte, Microcyte, Normal, Ovalocyte, Sickle Cell, Spherocyte, Stomatocyte, Target Cell, Teardrop Cell	98.5%
(Abdulkarim et al., 2020)	AlexNet	Over 9,000 single RBC images with 750 images for each type (650, 100)	Normal, Agglutination, Burr, Elliptical, Microcyte, Oval, unknown, Reticulocyte, Rolex, SC2, Triangle, Sickle, Stomatocyte, Macrocyte, Tear	95.92%
(Alzubaidi et al., 2020)	35 layer CNN + SVM	626 single RBC images	Normal, Sickle Cell, Others	99.98%

Author	Classification Method	Dataset (training, testing)	RBC Types	Result (Accuracy)
(de Haan et al., 2020)	2 U-net	96 patients with 9,630 RBCs	Normal, Sickle Cell	~98%
(Delgado-Ortet et al., 2020)	13 layer CNN	331 RBC images	Normal, Malaria	75.39%
(Rahman et al., 2021)	Rule-based	250 blood smear images	Normocyte, Microcyte, Macrocyte, Echinocyte, Acanthocyte, Elliptocyte, Sickle, Teardrop, Elliptic spur, Clump, Stomatocyte, Target, Hypochromic, Normochromic, Hyperchromic	97%
(Shakarami et al., 2021)	YOLOv3	364 blood smear images (3,943, 934)	RBC, WBC, Platelet	Mean average precision 89.86%
(Wong et al., 2021)	SVM, TabNet, U-	706 blood smear images with 20,926	Normal, Macrocyte, Microcyte, Hypochromia, Ovalocyte,	94.8%, 94.2%,

Author	Classification Method	Dataset (training, testing)	RBC Types	Result (Accuracy)
	net	single cells. (80%, 20%)	Schistocyte, Spherocyte, Sickle cell, Stomatocyte, Teardrop Cell, Target Cell, Burr Cell	78.2% F2-scores
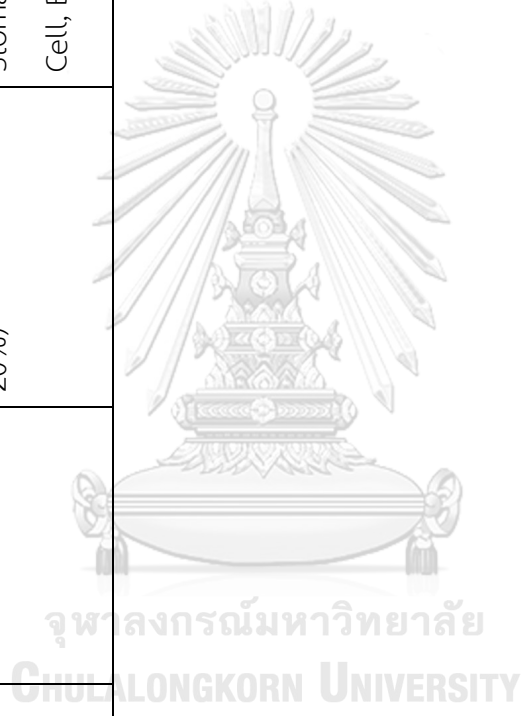
3. Related Theories

3.1. Red Blood Cell morphology

Red blood cell morphology (Ford, 2013) divides red blood cells into various subtypes by abnormalities of RBC shape, and other RBC features such as size, color, inclusion, and arrangement. Shape, size, and color features were focused on the classification method in this study. This thesis will not cover all the RBC types because each type can be found in different diseases, so some of RBC disorders are difficult to find in some regions making it hard to collect the data. The interested RBC types are described in Table 3-1.

Table 3-1 RBC type images and descriptions

Image	Description
	Normal cell The cell has a circular shape with circular central pallor.
	Macrocyte It like a normal cell but bigger.
	Microcyte It like a normal cell but smaller.

	Hypochromia Central polar is more than 1/3 the diameter of the RBC.
	Ovalocyte RBC with oval shape.
	Schistocyte It is a fragment of RBC. It usually shows another shape with no central pallor instead of a circular shape.
	Spherocyte The cell is smaller than normal. There is no central pallor.
	Sickle cell There are several sickle cell shapes. Generally, it looks like a boat, or crescentic with two sharp endpoints.
	Stomatocyte The central pallor is linear, rather than circular.
	Target cell The cell has a central area within the central pallor.

	Teardrop cell The shape looks like a drop of water.
	Burr cell The cell has serrated edges projection off its surface.

จุฬาลงกรณ์มหาวิทยาลัย

CHULALONGKORN UNIVERSITY

3.2. Ellipse Fitting

To estimate ellipse shape from a set of coordinate, (Aw Fitzgibbon & Fisher, 1995) proposed ellipse fitting algorithm minimizes an algebraic cost function on an ellipse equation

$$F(x, y) = ax^2 + bxy + cy^2 + dx + ey + f$$

With a constraint

$$b^2 - 4ac < 0$$

where x, y are the coordinate of each point and a, b, c, d, e, f are coefficients of the ellipse equation. This problem can be solved using the least-squares approach. The algorithm is well known and low resource computing. However, the algorithm can return a general conic shape, not specific on only the ellipse shape.

After that, (A. Fitzgibbon, Pilu, & Fisher, 1999) proposed a direct least-square fitting of the ellipse by adding a new constrain.

$$4ac - b^2 = 1$$

The new algorithm ensures that the result will be an ellipse even on the noisy set of points which is very robust.

3.3. Convolutional Neural Network (CNN)

The convolutional neural network was evolved from an artificial neural network that makes up of multiple neurons that have weights and biases. The architecture of the neural network is shown in Figure 3-1 consisting of an input layer, hidden layers, and an output layer. Each neuron receives values from the previous layer then performs a dot product follow by a non-linear function (optional). The data is put through the network called "forward propagation". After that, the network is trained by calculus-based called "back propagation" which learns how to correct the result comparing with ground truth.
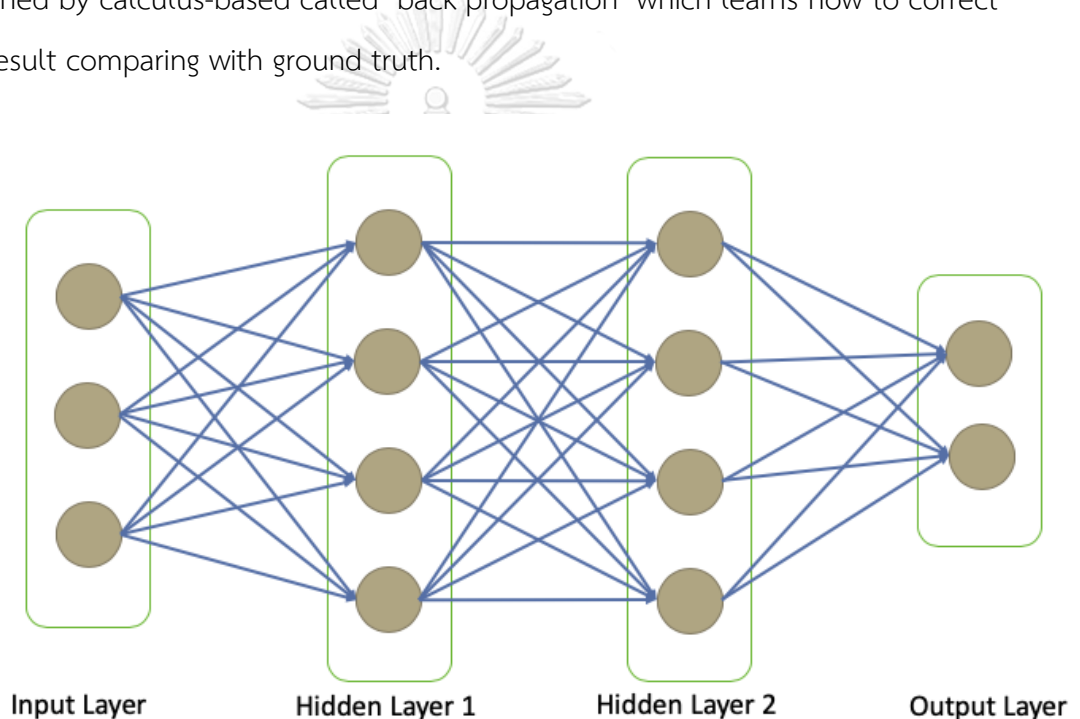
Figure 3-1 Artificial neural network

To implement image classification with the neuron network, the input layer is the set size of input neurons equal to the size of pixels of the image. In this case, the hidden layers will have a large number of neurons making it is computationally expensive. However, CNN solves this problem. CNN consists of 2 groups, feature

extractor layers, and fully connected layers. The architecture of CNN is shown in Figure 3-2.
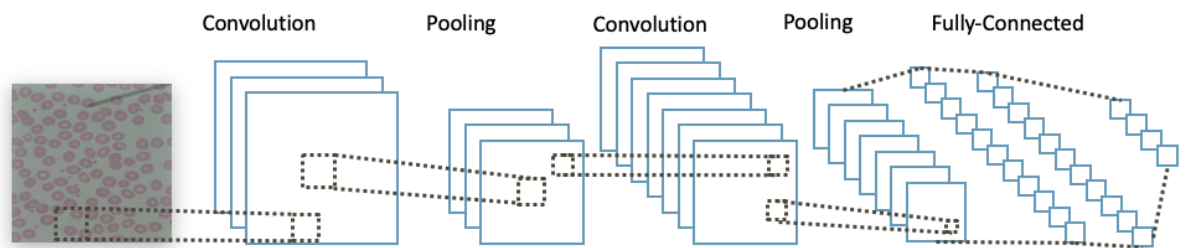

Figure 3-2 CNN architecture

The Feature extractor layers have 2 components, convolution, and pooling. Convolution is done by the dot product between each feature map and kernel then apply a non-linear function. The dot product is shown in Figure 3-3. Pooling is used to reducing the size of the feature map by reducing the layer size. There are two traditional types, max pooling, and average pooling. Pooling samples are shown in Figure 3-4.
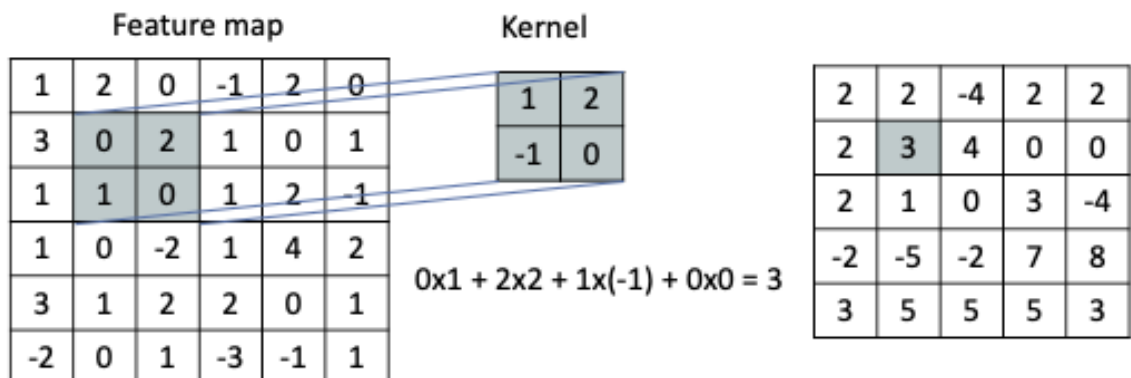

Figure 3-3 Sample of convolution between 6x6 feature map and 2x2 kernel
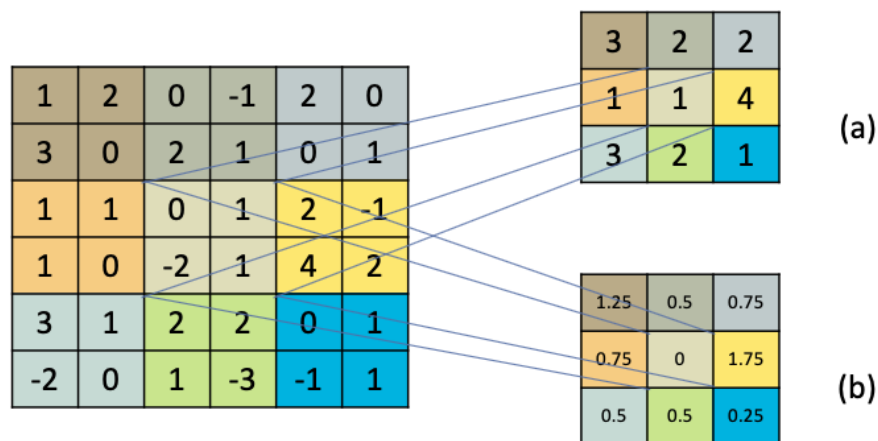
Figure 3-4 (a) 2x2 max pooling (b) 2x2 average pooling

The fully connected layers are the final step for predicting the result. This layer like the typical neural network which connects every neuron from the previous layer. For image classification, typically convolution and pooling are connected and repeated multiple times then a few fully connected layers are placed at the end which the last one has a size equal to the class size. In the early layer of convolution, each kernel detects low-level objects such as line, edge, curve, etc. In later layers, it will detect more complex objects. The CNN reduces computationally cost compare to the typical neural network because each kernel applies to all entire images to reduce unnecessary connections in the early layers and add more kernel making the network can go more in-depth instead.

3.4. Image Classification Model

3.4.1. AlexNet

AlexNet (Krizhevsky et al., 2012) was introduced to the world in 2012 with the winner in the ImageNet Large Scale Visual Recognition Competition (ILSVRC) which is an image classification competition. The AlexNet model outperformed all non-deep learning algorithms with a significant margin. The model has 8 layers, as shown in Figure 3-5. The convolution layers in this model are 11x11, 5x5, and 3x3 in dimension sizes. The total parameters to be trained are 60 million parameters. In addition, the ReLU activation function was introduced in AlexNet for the first time instead of TanH. The ReLU helps the model has to reach a lower error rate and also trains 6 times faster than TanH.
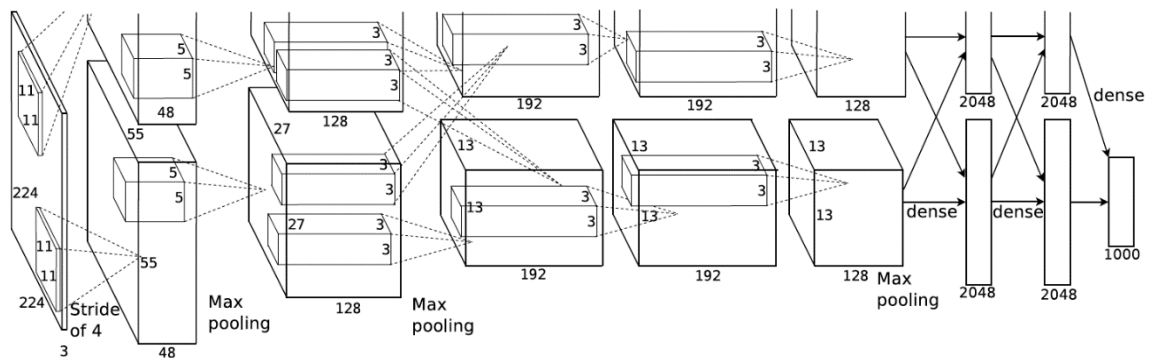

Figure 3-5 Architecture of AlexNet (Krizhevsky et al., 2012)

3.4.2. VGGNet

VGGNet (Simonyan & Zisserman, 2015) was introduced in 2014 as the winner in ILSVRC 2014. The VGGNet increases the number of model layers to 16 and 19, as VGG16 and VGG19 respectively. The model uses only 3x3 convolution layers instead of a larger convolution size because multiple 3x3 convolution layers have the same effect to one larger layer, but it needs fewer parameters to be trained. The total parameter for VGG16 is approximately 138 million parameters and for VGG19 is approximately 144 million parameters.
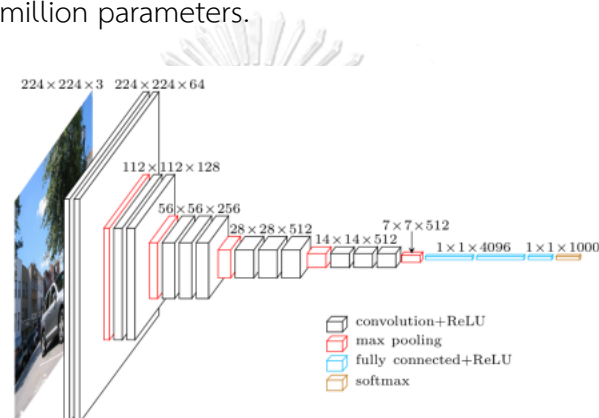

Figure 3-6 Architectures of VGG16 and VGG19 (Simonyan & Zisserman, 2015)

3.4.3. ResNet

ResNet (He et al., 2015) is the first CNN model that shows better than human performance. It was introduced as the winner in ILSVRC 2015 and COCO2015. Previous research had shown that the deeper CNN can achieve higher performance. However, training a model needs backpropagation. The gradients that pass through the deep model become smaller and show insignificant updates to the model, called the vanishing gradient problem. To handle this problem, ResNet uses the residual block, as shown in Figure 3-7, that adds a skip connection between the first layer of the block to the last layer of the block. These skip connections are the shorter paths to send back the gradient when backpropagation. The ResNet is a

connection of the residual block and it can go deep up to 150 layers, called ResNet152 which has 60 million parameters.
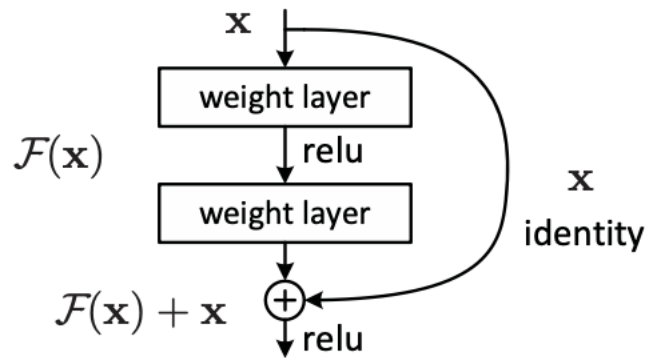

Figure 3-7 the Residual block in ResNet (He et al., 2015)

3.4.4. DenseNet

DenseNet (Huang et al., 2018) is a connection of dense blocks. Within the block, each layer connects to all previous layers, as shown in Figure 3-8. Instead of summing the previous layer like ResNet, DenseNet concatenates all previous feature maps, so the model does not need wide layers and it can reduce the number of feature maps. The DenseNet201, which has 201 layers, outperforms ResNet152 with fewer parameters and higher performance.
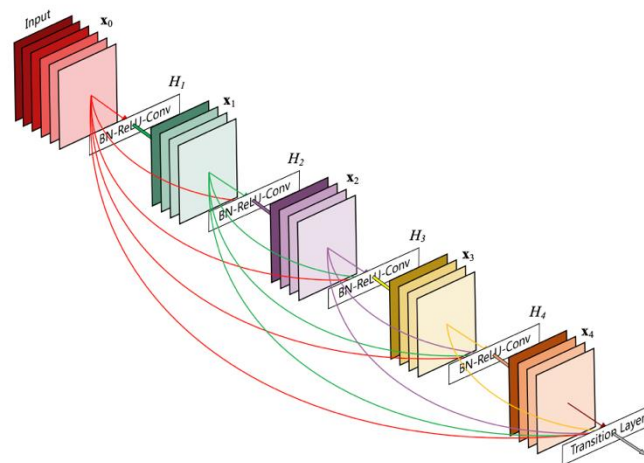
Figure 3-8 Dense block in DenseNet (Huang et al., 2018)

3.4.5. EfficientNet

Previous CNN architecture usually is a manual desired. EfficientNet was proposed with a set of models, EfficentNet-B0 – EfficientNet-B7, to fit a resource. Not only increase the deep layer of the model, the EfficientNet balances the width, depth, resolution of the model, as shown in Figure 3-9 using AutoML. The AutoML performs a grid search to find a relationship to scale the baseline network, which is mobile inverted bottleneck convolution (MBConv). For the performance, EfficientNet beats all previous models and also has lower computational power.
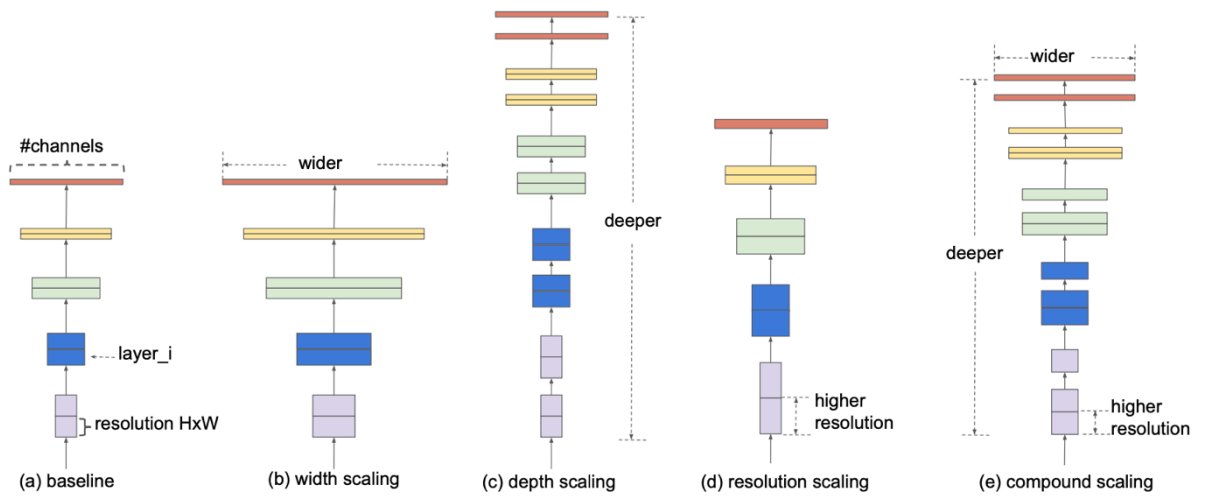
Figure 3-9 (a) is a baseline network, (b)-(d) show scaling in only one dimension, (e) compound scaling, including: wide, depth, and resolution, that was used in EfficientNet (Tan & Le, 2020)

3.5. Imbalance handling techniques

The most common problem for image classification in the medical area is an imbalanced dataset. Abnormal cases always have lower samples than normal cases. To handle the imbalance problem, several techniques have been invented to make the model does not bias to the majority classes. This section shows 3 methods that were used in this study to handle the imbalanced dataset.

3.5.1. Upsampling & downsampling

To handle the imbalanced dataset at the data level, all classes in the dataset should have samples equally. Downsampling decreases the sample in the classes that have many samples while upsampling increases the sample in the classes that have a low number of samples. It is easier to decrease the sample than to increase the samples. The augmentation technique is usually used to generate new samples.
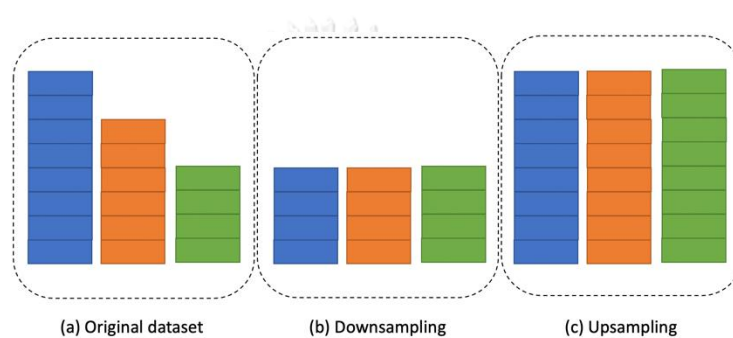

(a) Original dataset   (b) Downsampling   (c) Upsampling

Figure 3-10 (a) Imbalanced dataset (b) Downsapling technique that scales down the size of samples until equal to the lowest class (c) Upsampling technique that scales up the size of samples until equal to the highest class

3.5.2. Weight balancing

Weight balancing balances the training process in the loss function. Usually, the weight was assigned by the number of samples, low samples have higher weight, high samples have lower weight. The weights are multiplied with the loss to make the model less focused on the majority classes.

3.5.3. Focal loss

Focal loss is another weight balancing technique that was proposed in (Lin et al., 2018). First, it was used for object detection that the background class has much more pixels than the objects. However, it was modified to use in the image

classification task. The focal loss was modified from the cross-entropy loss, that commonly uses in image classification. The loss less focuses on the well-classified samples, as shown in Figure 3-11, making the model focuses on the sample with higher loss.
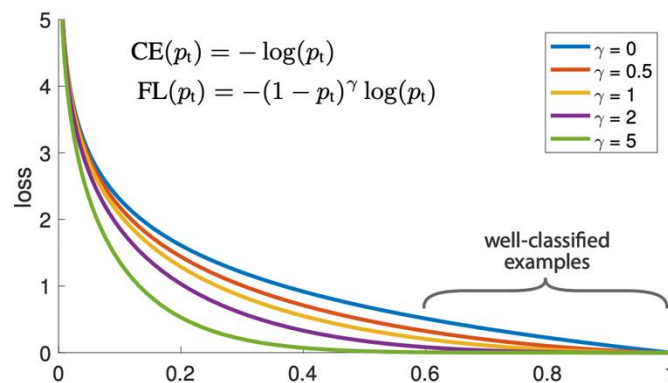

Figure 3-11 focal loss (Lin et al., 2018)

4. Proposed Methods

This chapter includes our data collection, normalization, segmentation, and classification. It covers a process from the blood smear is captured from a microscope to each RBC is classified to a type. The main contribution of this study is on data collection, segmentation, and classification. In data collection, we developed a software tool that helps experts label the RBCs. To the best of our knowledge, the dataset contains most classes of RBCs in the literature, and we plan to share this dataset to research community. In segmentation, a method for overlapping cell separation is proposed based on concave point findings. In classification, the EfficientNet model, which is the recent state-of-the-art for image classification, is employed.

Although, there have been many deep learning methods used for object detection, semantic segmentation, instance segmentation which are fully end-to-end learning based. However, the drawback of these methods is data preparation. To train the detection model, it needs bounding boxes and labels on every RBCs, but our dataset contains only some RBCs and coordinates. For these reasons, fully learning methods might not be suitable for this task.

4.1. Data collection

RBC images were collected from DS-Fi2-L3 Nikon microscope at 1000x magnification and were saved in the Google firebase database. After that, we have developed an IOS application for the specialist at the Faculty of Allied Health Sciences, Chulalongkorn university to label RBC in the images. It has two pages, a listed image view, and a labeled view, as shown in Figure 4-1.
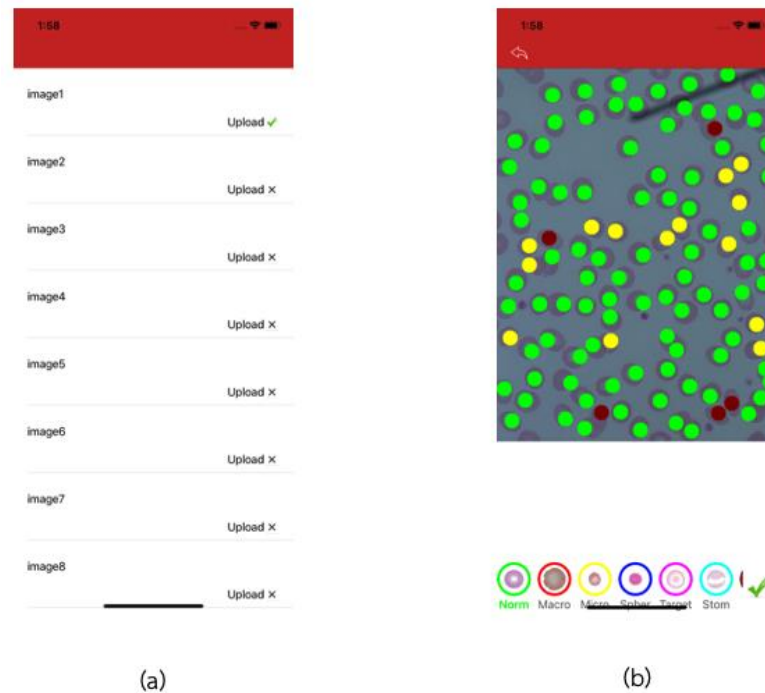
Figure 4-1 (a) Listed image view, (b) Labeled view

In the labeled view, users can select RBC types from the bottom of the screen then click on RBCs of that type in the image. The data will be automatically saved on Firebase. The data, which consists of x-y coordinate and type, were saved as JSON files which it can immediately use along with the labeling process. However, the abnormal RBCs that have an abnormality in shape can be identified with ease but the RBCs that have an abnormality in size are difficult. The blood smear images have a different scale when observed from the microscope, smartphone, and tablet. It is difficult to identify which cells are normal, microcyte, or macrocyte, even for a specialist. Ovalocyte is another type that needs to specify criteria, if the cells are slightly ellipse shape, it may confuse the labelers it is oval enough to be the ovalocyte. Moreover, in real-world situations, hematologists are not used tools to measure every cell in the slides, they usually use the experience to approximate the size of RBCs from the majority size of RBCs in the slides. But for labeling the ground truth. Every label needs to have an accurate label because the model in the image

classification problem does not have information from other cells, only a single-cell input. According to the normal RBCs, it has 6 - 8 microns. We have created a simple tool in our label application. The tool has 2 green circles which are calculated to have 6 and 8 diameters (16 and 22 pixels respectively) from the microscope reference scale. The tool is shown in Figure 4-2.
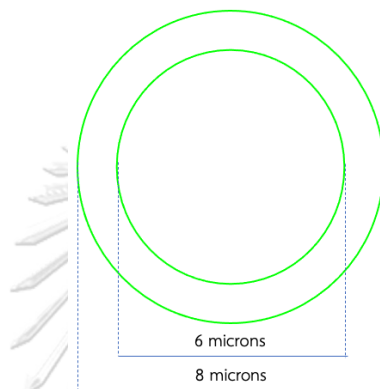
Figure 4-2 Circular shape tool for RBCs measurement

Labelers can move the tool to measure the cell along with marking the type of RBCs. The tool can help the labelers to measure 4 types: Normal cell, Macrocyte, Microcyte, and Ovalocyte by the rule in following.

- Normal cell: edge of the RBC needs to align between 2 circles.
- Microcyte: edge of the RBC needs to align inside the small circle.
- Macrocyte: edge of the RBC aligns outside the big circle.
- Ovalocyte: 2 opposite sides of RBC straight out of the big circle while another 2 opposite sides lie inside the big circle.

These rules can decrease confusion between each labeler. Before having this tool, labelers sometimes unsure whether the cell size is too big or too small comparing to the normal cell. The samples of the screen when classifying these 4 types are shown in Figure 4-3.
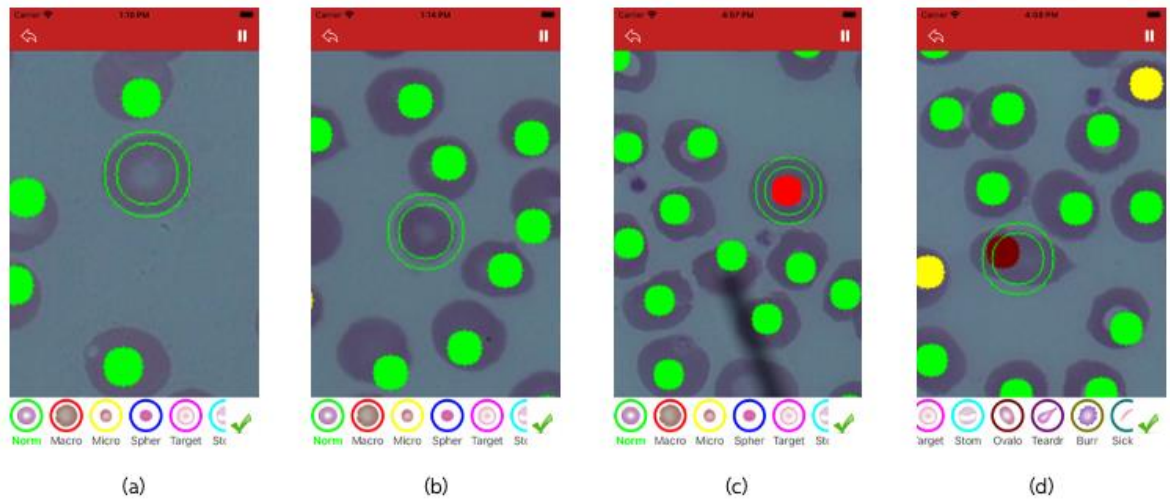
Figure 4-3 the circular shape tool in the mobile application for RBC measuring (a)
Normal cell, (b) Microcyte, (c) Macrocyte, (d) Ovalaocyte

In our experiment using dataset before using this tool explained in the next section, the confusion matrix showed that the majority of the wrong predictions are especially on Macrocytes and Microcytes. So, relabel process was done on the wrong prediction cells. To help the specialist to relabel with ease, we created an image with 3 components: a blood smear image with a rectangle box of the cell, an image from the rectangle box, and the rectangle box with no background and the circle tool. The type of the cell is shown in the lower left corner. Sample images were shown in Figure 4-4. The wrong labeling can happen in several causes. As shown in Figure 4-4 (a), the interesting cell seems smaller than other cells in the overall image so the specialist might think it is normal, but it is still Macrocyte. In Figure 4-4 (b), the interesting cell also seems smaller than other cells, but the majority is Macrocyte not Normal cell, so labeler assumed it was Microcyte instead of Normal cell. In Figure 4-4 (c), it is shown that the cell is small but also has an oval shape. For this reason, labelers need to agree to the labeling process because it cannot have 2 labels in 1 cell. The agreement is that abnormal RBC in shape is a priority than the second is

size. Similar to Figure 4-4 (c), it was relabeled as the Ovalocyte instead of the Microcyte.
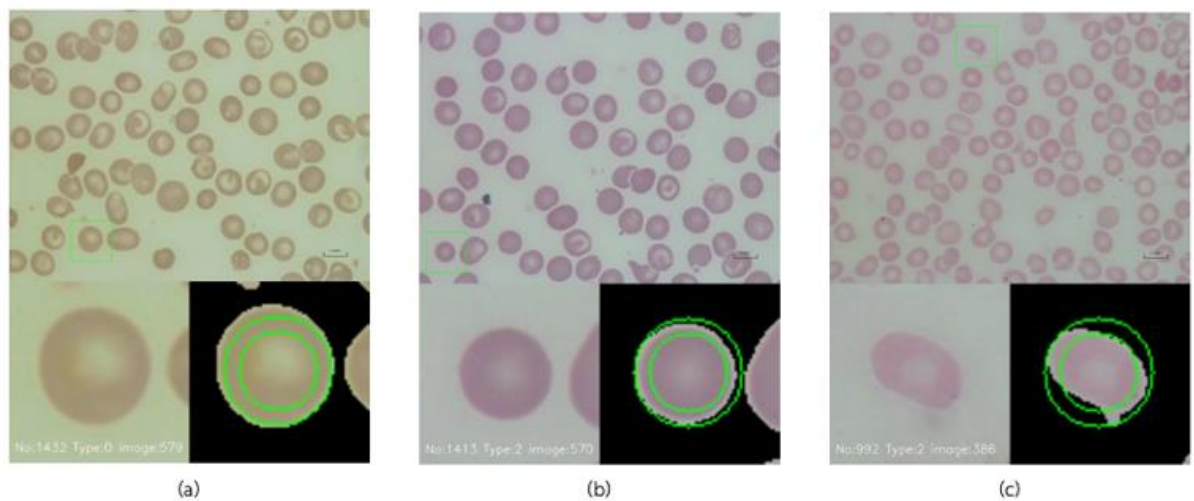
Figure 4-4 Sample images of relabel process. (a) Macrocyte was labeled as Normal cell, (b) Normal cell was relabeled as Microcyte, (c) Ovalocyte was labeled as Microcyte

The collection process did both blood smear image collection from the microscope and label the RBCs in parallel. The image collection timeline is shown in Table 4-1 and the label process timeline is shown in Table 4-2. As shown in the label process timeline, some types were decreased over time because the labeler relabeled the previous cells. The huge decreasing between 16/08/2019 and 06/09/2019 on Microcytes is because of a relabel process with the circle tool recorrect Microcyte as Normal cell.

Table 4-1 Timeline of blood smear image collection

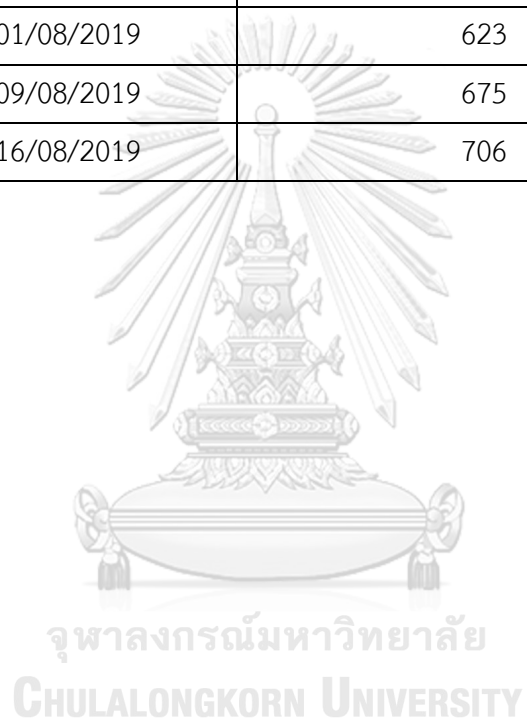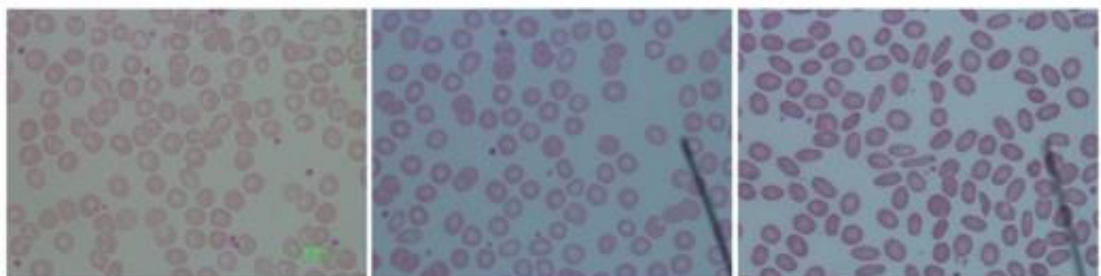| Date	Number of blood smear images
13/12/2018	231
20/03/2019	285
30/03/2019	389
20/06/2019	492
16/07/2019	559
31/07/2019	583
01/08/2019	623
09/08/2019	675
16/08/2019	706

Table 4-2 Timeline of labeling process

| Type/Date	27/3/2019	28/3/2019	1/4/2019	2/4/2019	18/4/2019	25/4/2019	5/5/2019	12/7/2019	31/7/2019	15/8/2019	16/8/2019	06/09/2019
Normal cell	4,841	4,854	5,084	5,101	5,523	5,559	5,423	5,485	5,481	5,875	5,876	6,286
Macrocyte	1	1	12	144	141	136	140	218	351	622	646	687
Microcyte	38	38	220	513	548	573	879	884	950	1,254	1,253	459
Spherocyte	562	1,298	1,821	2,070	2,113	2,117	3,406	3,410	3,422	3,465	3,467	3,445
Target cell	1,439	1,579	1,674	1,723	1,766	1,766	2,032	2,077	2,246	2,674	2,690	2,703
Stomatocyte	54	54	55	110	1,919	1,920	1,939	1,947	1,947	1,950	1,950	1,991
Ovalocyte	502	505	604	806	1,334	1,337	1,719	1,729	1,788	2,047	2,051	2,137
Teardrop cell	38	44	49	53	54	54	68	160	220	240	240	305
Burr cell	248	289	419	435	436	436	502	502	630	642	695	783
Sickle cell	5	5	5	4	4	4	4	4	4	4	4	4
Schistocyte	174	183	257	335	368	368	397	481	713	778	783	861
Uncategorized cell	939	2,474	637	212	209	209	109	109	109	266	266	182
Hypochromia	124	124	173	204	338	340	613	617	619	876	876	1,036
Polychromasia					9	15	22	23	23	32	34	37
Keratocyte					1	1	3	3	4	5	5	4
Acanthocyte					0	0	4	4	6	7	7	6
Total	8,965	11,448	11,010	11,710	14,763	14,835	17,260	17,653	18,513	20,737	20,843	20,926

4.2. Normalization

In our blood smear dataset, as shown in Figure 4-5, the images are different in light conditions. Collectors might have different environments, such as camera settings, microscope light levels, blood smear slide preparation, etc. It can happen by multiple causes: such as the brightness of light in the microscope, camera settings, substances that using in slide preparation, or even light from the environment. The collectors also might collect multiple blood smear slides of a single RBC type at a time, making each type have its own color space. Although hematologists can disregard the difference in color space from expertise, the model can be biased from the different color spaces during the training process instead of the characteristics of that type. Hence, normalization is needed to preprocess the images before classification.

Figure 4-5 Samples of blood smear images
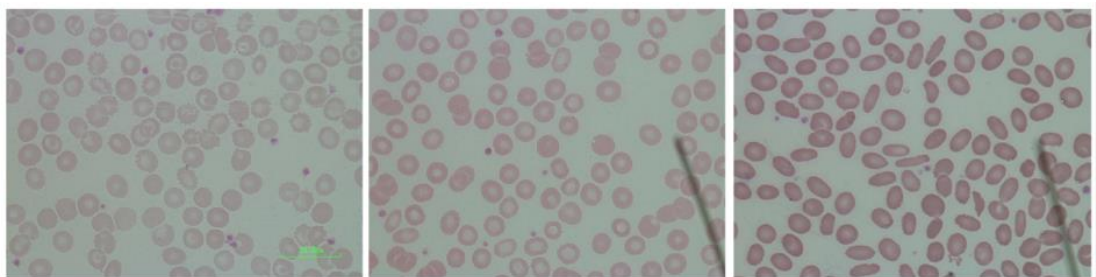
Figure 4-6 Samples of blood smear images after normalization

In this step, the backgrounds were extracted and the three overall average background values of the RGB channels (R_{avg}, G_{avg}, and B_{avg}) were found for all the blood smear images. Before training and predicting the results, the different values of the three average background values of the target image k and the overall averages values were added to all the pixels of the target image. The normalization equation of pixel (i, j) for image k is shown in the equation below. Although only the normalized images were used for improving the classification results, a huge improvement in the normalization accuracy was found. The results are shown in Figure 4-6.

$$r^k_{i,j} = r^k_{i,j} + \left(R_{avg} - r^k_{avg}\right)$$
$$g^k_{i,j} = g^k_{i,j} + \left(G_{avg} - g^k_{avg}\right)$$
$$b^k_{i,j} = b^k_{i,j} + \left(B_{avg} - b^k_{avg}\right)$$

4.3. Segmentation

In this step, the segmentation was done for extracting the RBC area as contours out of the background. It starts with preprocessing the image. First, the image was converted to greyscale by selecting the green channel of the RGB image. It was selected because the green channel has more contrast than the red and blue channels. The RBCs have purple red color making the green channel has a lower value while the background contains a high value on all 3 channels. As shown in Figure 4-7, (a) shows the RBC sample image and (b) – (d) show R, G, and B channels, respectively. (e) shows a histogram of the RBC color of the image (a). It was shown that each channel has 2 peaks, the higher peak always has a higher value due to the background and the lower peak is the RBC area. The farthest distance between the 2 peaks is on the green channel making it has the highest contrast compared with all 3 channels.

(a)

(b)

(c)

(d)
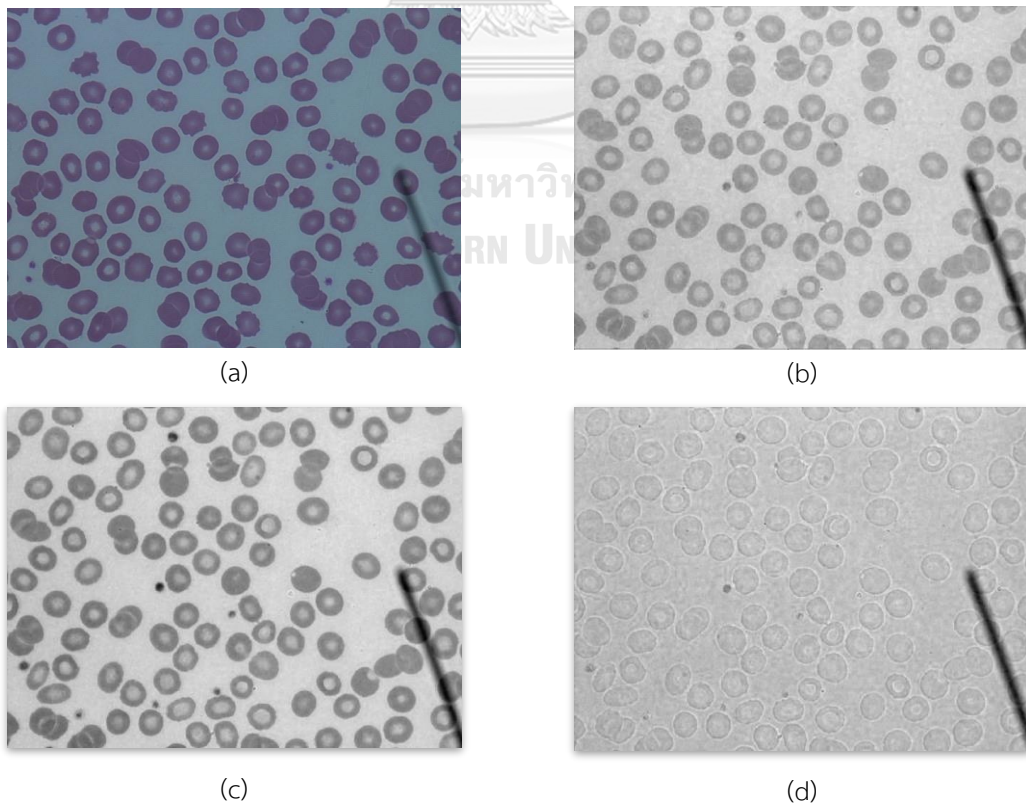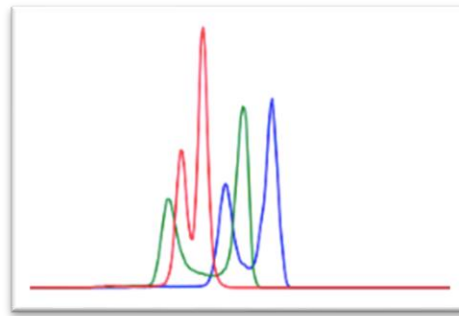
(e)

Figure 4-7 (a) RBC original color image. (b) Image from the red channel. (c) Image from the green channel. (d) Image from the blue channel. (e) Histogram of RGB color.

Next, CLAHE (Contrast Limited Adaptive Histogram Equalization) was used to enhance the image. The grayscale was divided into small blocks (8x8). The small blocks were done histogram equalization separately, as shown in Figure 4-8. Blur and threshold were used to extracting the cell area out of the background. The steps are shown in Figure 4-8 (c) – (d).

(a)   (b)

(c)

(d)
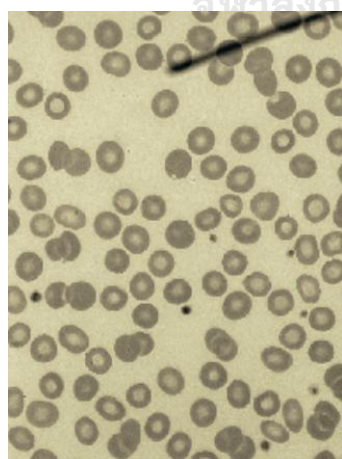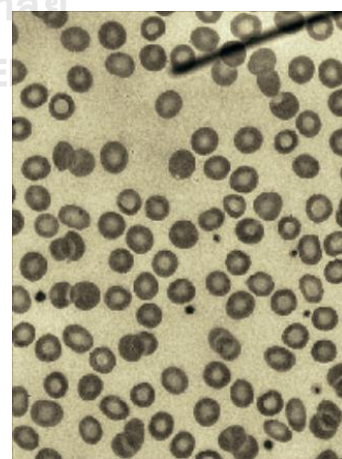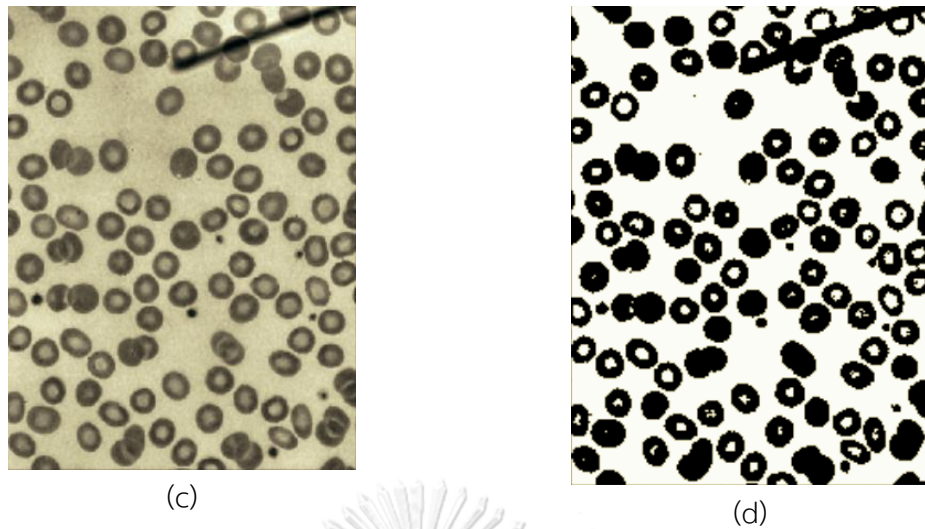
Figure 4-8 (a) Green channel image. (b) CLAHE image. (c) Blur image. (d) Threshold

image

After that, we need to extract the edges of each cell by extracting the contour using morphology operation. The output is contours of ROI regions contains coordinates of the border. Finding a closed area was used as shown in Figure 6-5.

Figure 6-5 Closed area image

4.4. Overlapping separation

In manual RBC analysis, hematologists typically avoid selecting an area in a blood smear slide that has overlapping cells to evaluate the result. This is because it is simple to count and identify the type of RBC when their border is not hidden beh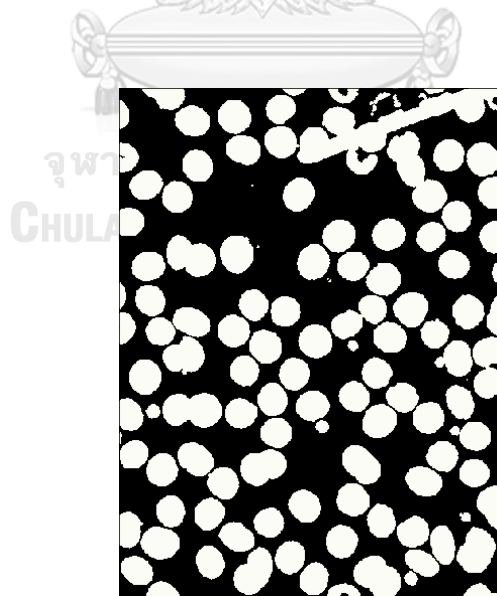ind other cells. To separate the overlapping RBCs, the most reliable methods are based on distance transforming and ellipse fitting. The distance transform approach is used to find the peak spots furthest from the border. The peak spots are then used to identify a unique cell by several techniques, such as the random walk method and watershed transform, and the area of each cell was found. However, although the distance transform works effectively for a circular shape and a small group of overlapping cells, the peak area may coexist making it difficult to specify a certain amount. The ellipse fitting method uses the edge of the RBC to approximate as an ellipse which identifies the area of RBC.

The method presented herein is based on ellipse fitting and the overall process was divided into four steps, as detailed below. The steps are shown in Figure 4-11.

4.4.1. Concave point finding

In each point (coordinate) in the RBC contour, (x_i, y_i), k middle points were calculated by finding the center of the distance between k pairs of contour points near the point. If all k points are outside the contour, the point is considered as a concave point, as shown in Figure 4-9. However, when more than one concave point can be found in a wide curve, as shown in Figure 4-11 (b), only one concave point was selected by averaging all near concave points. The concave points function, $f(x)$, was calculated using Equation (4.1) and (4.2).

$$f(x_i, y_i) = \prod_{j=1}^{k} g(\frac{x_{i-j} + x_{i+j}}{2}, \frac{y_{i-j} + y_{i+j}}{2}) \qquad (4.1)$$

$$g(x) = \begin{cases} 1, (x, y) \text{ is outside a contour} \\ 0, (x, y) \text{ is inside a contour} \end{cases} \qquad (4.2)$$
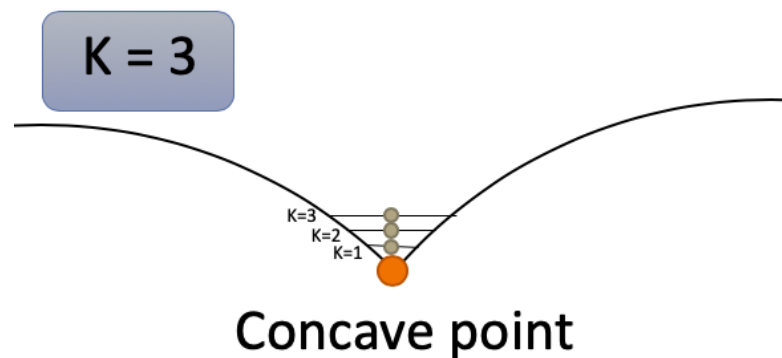
Figure 4-9 Concave point finding

4.4.2. Ellipse estimation

If the contour has more than one concave point, curves between the two concave points were used to approximate an ellipse shape by direct ellipse fitting (A. Fitzgibbon et al., 1999), based on the least-square method. The direct ellipse fitting is recommended instead of the original (Aw Fitzgibbon & Fisher, 1995), which gives an approximate ellipse that does not relate to the curve in some conditions. The direct ellipse fitting is constrained by ensuring the discriminant $4ac - b^2 = 0$ for the ellipse equation. The Figure 4-10 shows the incorrect results of the original ellipse fitting comparing with the direct ellipse fitting.
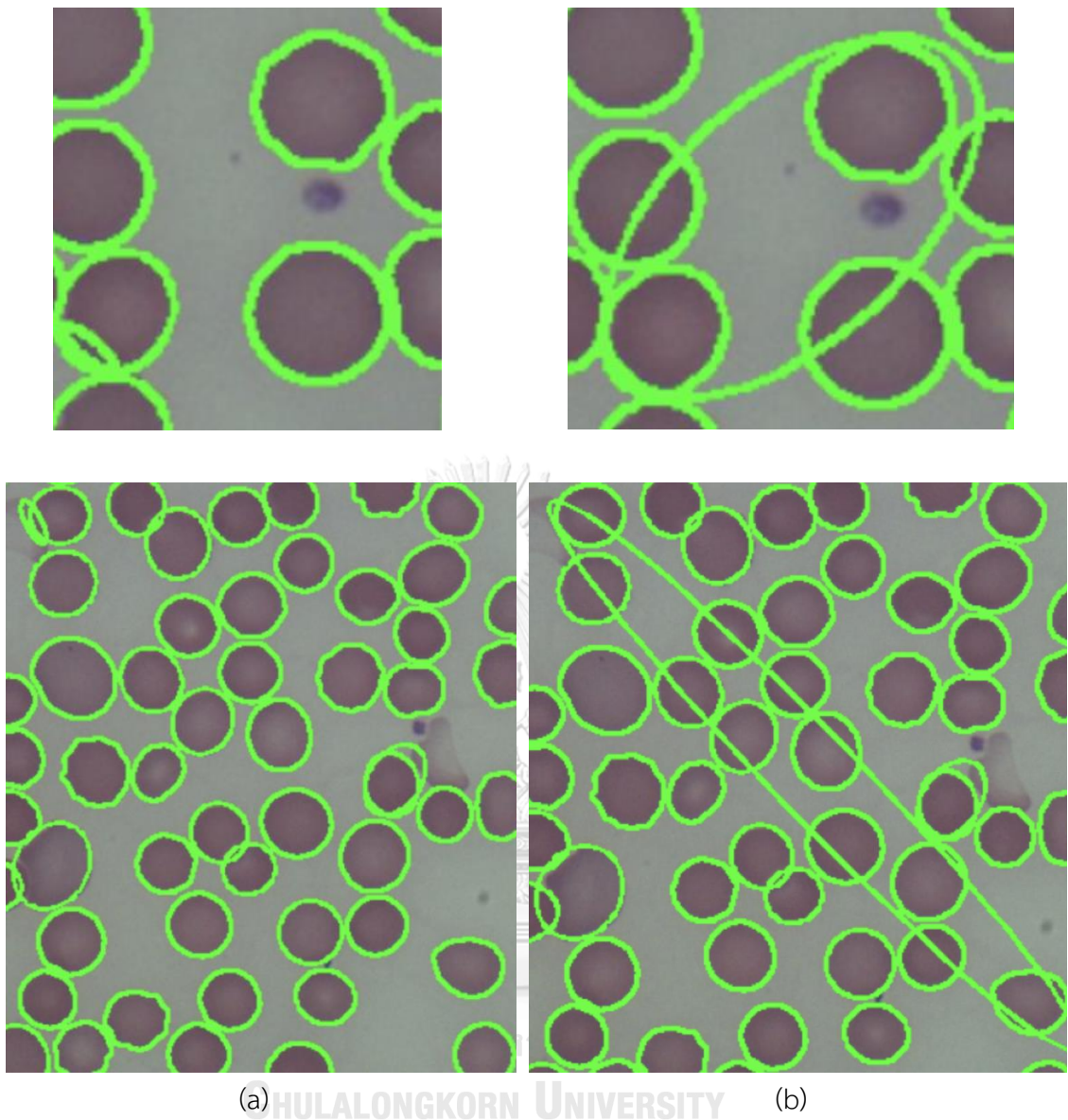
Figure 4-10 (a) shows results of the direct ellipse fitting, (b) shows results of the original ellipse fitting

4.4.3. Ellipse verification

After finding all the ellipses in each contour, the ellipses were sorted by area in descending order. Then, each ellipse was verified to be in the RBC contour by meeting two simple conditions of (i) 80% of the ellipse area is in the contour and (ii) 20% in the remaining area in the contour is not in any previous ellipses.

4.4.4. Two curve ellipse estimation

In highly overlapping RBCs, more than two cells overlap each other and so the curves might not be able to restore the correct ellipse shape of each RBC. If there are more than two ellipses that do not pass the conditions, then the two curves were concatenated and used to estimate an ellipse of the remaining cell.
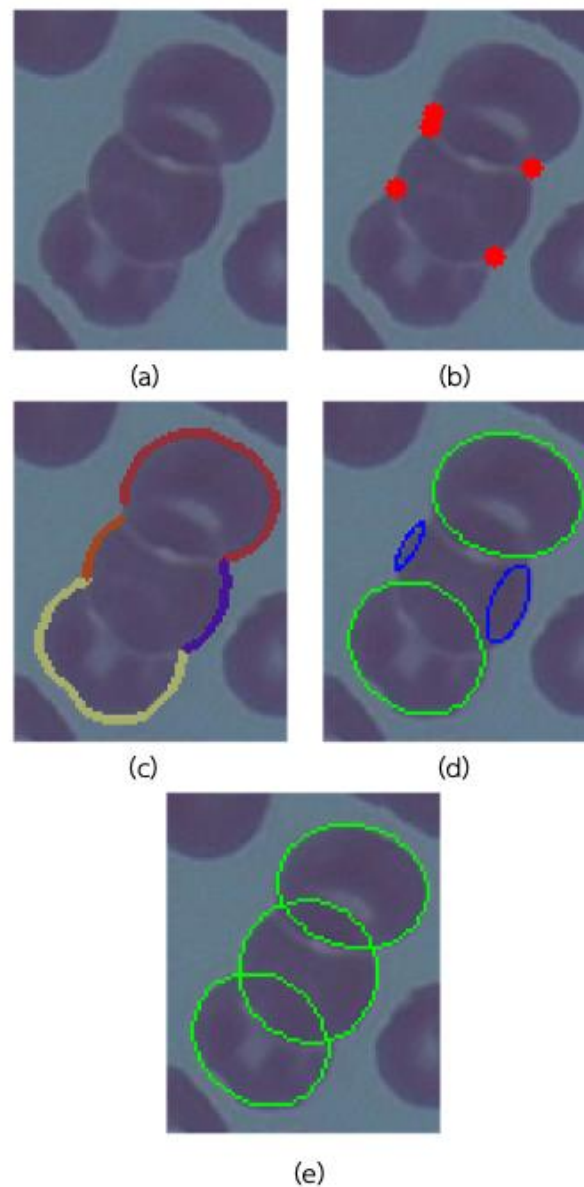
Figure 4-11 Steps in the overlapping cell separation: (a-c) two curves are concatenated and used to estimate an ellipse of the remaining cell. (d) The two

blue ellipses show an incorrect cell estimation, while (e) shows the correct cell estimation after ellipse fitting with two curves.

4.5. Classification

4.5.1. RBC dataset

After the segmentation step, single RBC contours are extracted out of the blood smear images. To feed to the CNN model, single RBC images are created. The RBC contour are put in the middle of the output image, as shown in Figure 4-12. After that, the images are resized to 224x224 pixels which is the default size that the original work using.

The dataset had 12 classes of RBCs: 11 RBC types and an uncategorized class, which is other type of RBC. The dataset was labeled by specialists in hematology. The numbers of RBCs in each class are shown in Table 4-3. The dataset is highly imbalanced because some classes are rare, such as the Teardrop, Sickle cell, and Uncategorized types. However, in data collection process, we have collected the Sickle cell, Polychromasia, Keratocyte, and Acanthocyte. These 4 RBC types still have small number of samples which is not enough for training.
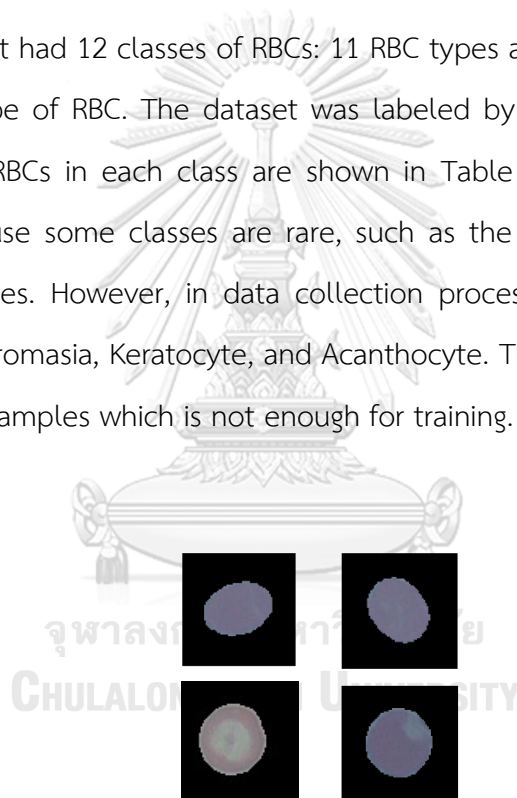
Figure 4-12 Samples of single RBC images before feeding to the deep learning model

Table 4-3 Total number of each RBC class in the dataset

RBC Class	Total number of RBCs
Normal cell	6,286
Macrocyte	687
Microcyte	459
Spherocyte	3,445
Target cell	2,703
Stomatocyte	1,991
Ovalocyte	2,137
Teardrop cell	305
Burr cell	783
Schistocyte	861
Uncategorized cell	182
Hypochromia	1,036
Total	20926

4.5.2. Classification model

For classification, the pretrained EfficientNet model (Tan & Le, 2020) was used as it showed a remarkable level of accuracy and better performance than the older models. It was designed by carefully balancing the network depth, width, and resolution. The model has eight different sizes: EfficientNet-B0 to EfficientNet-B7. In the results section, the EfficientNet-B0 to EfficientNet-B4 were observed with a five-fold cross validation using 80% and 20% for training and testing, respectively.

4.5.3. Augmentation

The data augmentation will be used for this problem. It can generate new data by applying a function to the data. Only random flips and rotates were used

for data augmentation because the RBC classes are sensitive to size and color, such as Normal Macrocytes and Microcytes are different in size.

4.5.4. Imbalanced handing techniques

Further analysis on the imbalanced dataset was then performed an imbalanced dataset is a common problem in biomedical datasets. Our RBC dataset was highly imbalanced with a 34.538 imbalance ratio (calculated from highest sample class/lowest sample class) for the 12 RBC classes from a total of 20,875 RBCs. In the training step, the model can be overcome by high sample classes with less focus on the low sample classes. Thus, the weight balancing, up sampling, and focal loss were investigated in this study.

For weight balancing, normally, every RBC class has the same weight, 1.0. However, the weight balancing helps a model balances learning gradients in the backpropagation step between high sample classes and low sample class, by giving a high weight to low sample classes and a low weight to high sample classes. In this study, each class was weighted as $\frac{1}{f}, \frac{1}{\sqrt{f}}, \frac{1}{\sqrt[3]{f}}$ as weights 1, 2, and 3, respectively, where f is the number of samples in that class.

The up sampling makes every RBC class have the same number of samples by replicating its own data. This helps the trained model to not be overcome by high sample classes. In this case, every class replicates itself to match the normal class.

For the focal loss, as shown in the Figure 3-11 focal loss , the γ parameter adjusts how the loss function less impact on well-classified samples, higher γ less impact on well-classified samples. 0.5, 1.0, 1.5, 2.0 ,2.5, 3.0 were used in the γ parameter in our test.

4.5.5. Evaluation metric

To evaluate the performance, accuracy is commonly used for image classification. For the imbalanced dataset, the accuracy is insufficient, as it can be dominated by the majority classes. However, many metrics have been used to describe an imbalanced dataset (Johnson & Khoshgoftaar, 2019), and the F1-score was used in this study. This is a well-known metric that balances precision and recall by harmonic means that is sensitive to the minority classes. Normally, for binary classification, precision, recall, sensitivity, specificity, and F1-score were used to evaluate the result in imbalance dataset. In contrast, multi-class classification multiple metrics are hard to compare.
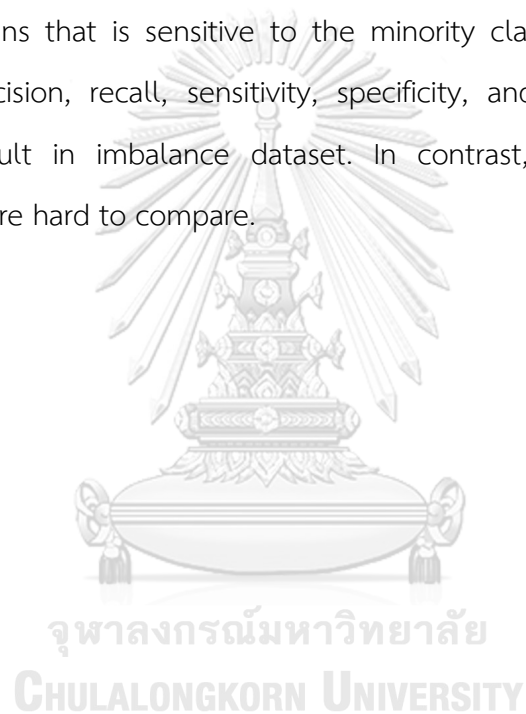
5. Experimental Results

5.1. Overlapping cell separation

In this section, overlapping cell separation performance was tested in 20 blood smear images. We manually counted the overlapping contours that did not contain a cell on the border of the images and other artifacts, such as platelets, white blood cells, or microscope tools in the images. A total of 277 contours were found. Our algorithm can correctly separate 246 overlapping cells which are 0.8881 accuracies. The incorrect results include undetected overlapping cells, and the result does not fit the true shape of RBCs. According to the wrong results, it can happen in incorrect concave point finding and incorrect ellipse fitting. The results are shown in Table 5-1. Mostly found in the blood smear images are the two overlapping cells. The incorrect results mostly are caused by wrong concave point findings.

Table 5-1 Overlapping cells separation result

Contour	Correct	Incorrect (Concave)	Incorrect (Fitting)	Total
2 RBCs	185	18	4	207
3 RBCs	38	2	1	41
> 4 RBCs	23	2	4	29
Total	246	22	9	277

In Figure 5-1, the incorrect overlapping cell separations are shown. (a) is incorrect because only one concave point is found, (b) and (c) are incorrect due to incorrect ellipse fitting. In Figure 5-2, the correct overlapping cell separations are shown. (a) and (b) are simple overlapping cells, while (c) is a complex group of overlapping cells.
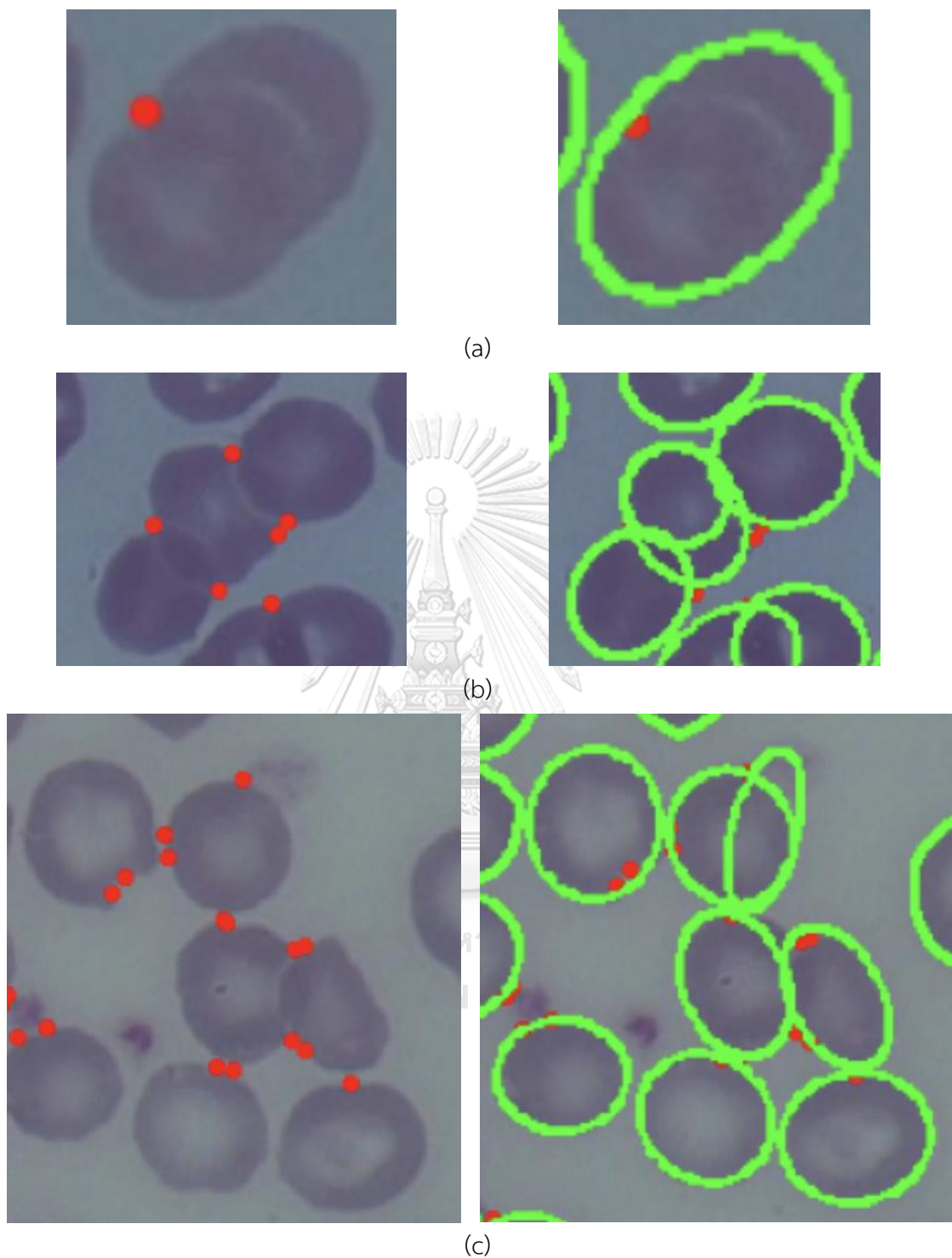
Figure 5-1 (a) shows incorrect overlapping cell separation because of incorrect concave point finding (b)-(c) show incorrect ellipse fitting because of incorrect ellipse fitting

(a)

(b)

(c)
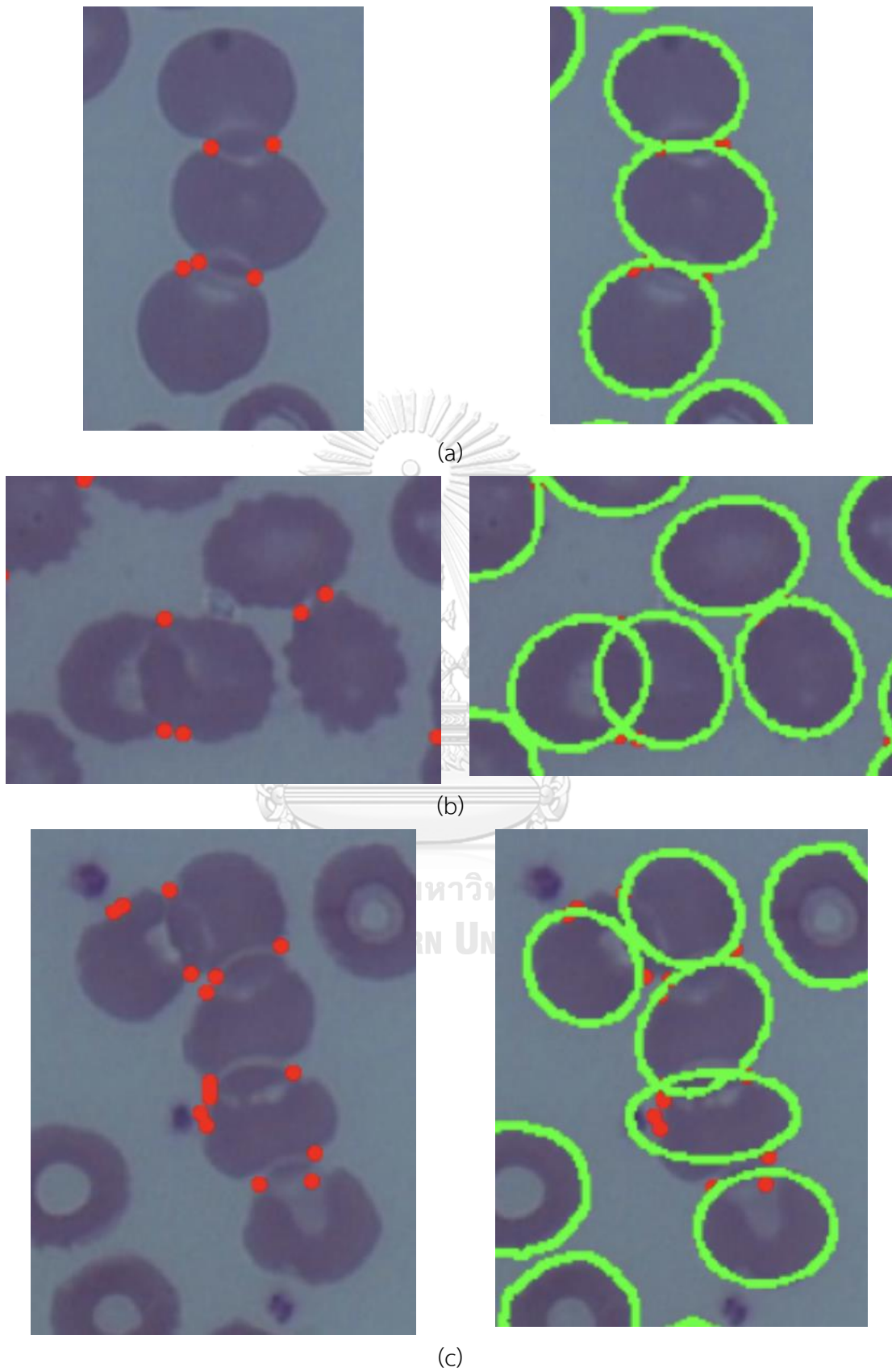
Figure 5-2 (a)-(c) show correct overlapping cell separation

5.2. RBC Classification

In the first step, we investigated the different model sizes, EfficientNet-B0 to B4, with and without augmentation. The results (Table 5-2) show that EfficientNet-B1 with augmentation had the highest accuracy and F1-score. Thus, increasing the model size did not significantly improve the performance, and the limiting factor was the sample size of the dataset. Increasing the model size can then lead to an overfitting problem. Therefore, imbalance handling techniques were investigated, including weight balancing, up sampling, and focal loss, using EfficientNet-B1 as the baseline.

Table 5-2 RBC classification results

Model	Accuracy	F1-score
EfficientNet-B0	0.8821	0.8378
EfficientNet-B1	0.8823	0.8426
EfficientNet-B2	0.8842	0.8399
EfficientNet-B3	0.8819	0.8423
EfficientNet-B4	0.8830	0.8405
EfficientNet-B0-aug	0.8996	0.8639
EfficientNet-B1-aug	**0.9021**	**0.8679**
EfficientNet-B2-aug	0.8988	0.8636
EfficientNet-B3-aug	0.9001	0.8642
EfficientNet-B4-aug	0.8990	0.8668

The overall training accuracy and F1-score of EfficientNet-B1 with imbalance handling techniques are summarized in Table 5-3. However, the baseline model with augmentation still had the highest accuracy and F1-score, followed by AugWeight3 (augmentation and $\dfrac{1}{\sqrt[3]{n}}$ weight). Up (Up sampling) showed a slightly lower result

from the baseline while AugUp (Augmentation with up sampling) showed slightly better results. Augmentation with focal loss (AugFocal0.5-AugFocal3.0) resulted in a decreasing accuracy and F1-score with increasing γ hyperparameter values.

Table 5-3 Accuracy and F1-Score of our proposed EfficientNet-B1 with various data imbalance handling techniques

Model	Accuracy	F1-score
Baseline	0.8823	0.8426
Aug	**0.9021**	**0.8679**
Weight	0.8752	0.8374
Weight2	0.8808	0.8435
Weight3	0.8820	0.8410
AugWeight	0.8698	0.8344
AugWeight2	0.8954	0.8630
AugWeight3	0.8981	0.8672
Up	0.8772	0.8403
AugUp	0.8877	0.8591
AugFocal0.5	0.8947	0.8523
AugFocal1.0	0.8932	0.8510
AugFocal1.5	0.8926	0.8543
AugFocal2.0	0.8900	0.8480
AugFocal2.5	0.8884	0.8486
AugFocal3.0	0.8877	0.8488

The average results in the imbalanced handing techniques might not tell much about the performance of the model. In Table 5-4, F1-scores of each technique in classes are shown. The augmentation row is highlighted, and the bold values are shown that they are better than the augmentation in that class. The

weight balancing with augmentation shows better F1-score on low sample classes, AugWeight2 and AugWeight3 have 4 and 6 classes better than only augmentation. The upsampling with augmentation has 3 classes better than the augmentation. The result in Table 5-4 shows that the weight balancing with augmentation technique can help the model focusing on the low sample classes. The reason that the overall F1-score still lower than the augmentation technique because our dataset is highly imbalanced, the lowest which is uncategorized and teardrop cell have 182 and 305 samples while the normal has 6,286 samples.

In summary, the difference between this dataset and general datasets in the RBC classification problem are the dataset is imbalanced and RBC classes have many similar characteristics. Almost all classes are circular in shape, with only a few characteristics that are different, such as their size, shape, and color. The best result was obtained with the EfficientNet-B1 with augmentation.

Further analysis on an imbalanced dataset, weight balancing, and focal loss were examined for their effect on the loss function. Weight balancing helped to improve the low sample classes with less focus on the high sample classes. Otherwise, focal loss showed a decreased performance for this dataset because it focused on a high value loss, but since the different RBC classes were almost similar in shape the loss was almost entirely in the middle, which is ignored. Up sampling was performed at the data level, similar to augmentation. This technique seemed to work best for unique shape classes, which were the teardrop cell and uncategorized classes.

The further experiment on background color for feeding into the model was done, as shown in Table 5-5. Normally the black background was used in the experiment. The experiment was done with black background, white background, gray background, and average background from the blood smear image background. The result shows that the black background has the best performance.

The normalize RBC techniques also was tested, the first row of Table 5-5. The result has very low performance because our blood smear images have variance of background color. The blood smear image collector may collect the images type by type, so each type has their own environment of lighting. For this reason, the normalization needs to be done before feeding to the model.

In Figure 5-3, samples of segmentation and classification are shown. The number near each cell shows the number of predicted RBC types. The number is in Table 5-6

Table 5-4 F1-score of classifying RBCs classes using EfficientNet-B1 with data imbalance handling techniques

Techniques	Normal	Macrocyte	Microcyte	Spherocyte	Target cell	Stomatocyte	Ovalocyte	Teardrop	Burr cell	Schistocyte	Uncat	Hypochromia
Baseline	0.8811	0.8176	0.6543	0.9311	0.9347	0.8996	0.8899	0.8188	0.8567	0.8126	0.8466	0.7684
Aug	0.9023	0.8487	0.6850	0.9456	0.9408	0.9168	0.9128	0.8840	0.8783	0.8528	0.8499	0.7980
Weight	0.8719	0.8131	0.6675	0.9279	0.9256	0.8879	0.8866	0.8060	0.8658	0.8090	0.8323	0.7549
Weight2	0.8763	0.8308	0.6417	0.9331	0.9319	0.8967	0.8942	0.8200	0.8654	0.8052	0.8604	0.7664
Weight3	0.8804	0.8205	0.6439	0.9312	0.9333	0.9051	0.8947	0.8258	0.8495	0.8178	0.8333	0.7568
AugWeight	0.8500	0.7919	0.6210	0.9295	0.9348	0.9020	0.9025	0.8685	0.8614	0.8364	0.7527	0.7626
AugWeight2	0.8900	0.8267	0.6888	0.9423	0.9422	0.9169	0.9089	0.8738	0.8753	0.8441	0.8485	0.7991
AugWeight3	0.8943	0.8282	0.6798	0.9407	0.9426	0.9183	0.9118	0.8936	0.8814	0.8552	0.8626	0.7974
Up	0.8787	0.7946	0.6036	0.9286	0.9336	0.8867	0.8910	0.8644	0.8228	0.8098	0.9014	0.7681

AugUp	0.8874	0.7934	0.6519	0.9385	**0.9417**	0.8873	0.9047	**0.9244**	0.8418	0.8294	**0.9296**	0.7794
AugFocal0.5	0.8928	0.8337	0.6389	0.9394	**0.9430**	0.9162	0.9112	0.8591	0.8736	0.8293	0.8047	0.7852
AugFocal1.0	0.8925	0.8237	0.6529	0.9409	0.9399	0.9101	0.9067	0.8346	0.8738	0.8383	0.8205	0.7777
AugFocal1.5	0.8889	0.8310	0.6648	0.9368	**0.9424**	0.9101	0.9114	0.8532	0.8734	0.8343	0.8264	0.7788
AugFocal2.0	0.8873	0.8250	0.6689	0.9395	0.9372	0.9112	0.9086	0.8538	0.8674	0.8201	0.7900	0.7669
AugFocal2.5	0.8837	0.8272	0.6753	0.9366	0.9401	0.9015	0.9118	0.8490	0.8583	0.8312	0.8038	0.7649
AugFocal3.0	0.8834	0.8199	0.6635	0.9371	0.9355	0.9014	0.9048	0.8376	0.8741	0.8215	0.8238	0.7825

Table 5-5 Accuracy and F1-score of EfficientNet-B1 with different normalization techniques

Model	Accuracy	F1-score
AugUnnormalize	0.6325	0.4241
AugBlackbg	0.9021	0.8679
AugWhitebg	0.8977	0.8634
AugGraybg	0.8969	0.8603
AugAVGbg	0.8979	0.8626

Table 5-6 Average Precision, Recall, and F1-score of five-fold cross validation using our method on Yale's dataset

Number of RBC types	RBC types
0	Normal cell
1	Macrocyte
2	Microcyte
3	Spherocyte
4	Target cell
5	Stomatocyte
6	Ovalocyte
7	Teardrop cell
8	Burr cell
9	Schistocyte
10	Uncategorized cell
11	Hypochromia
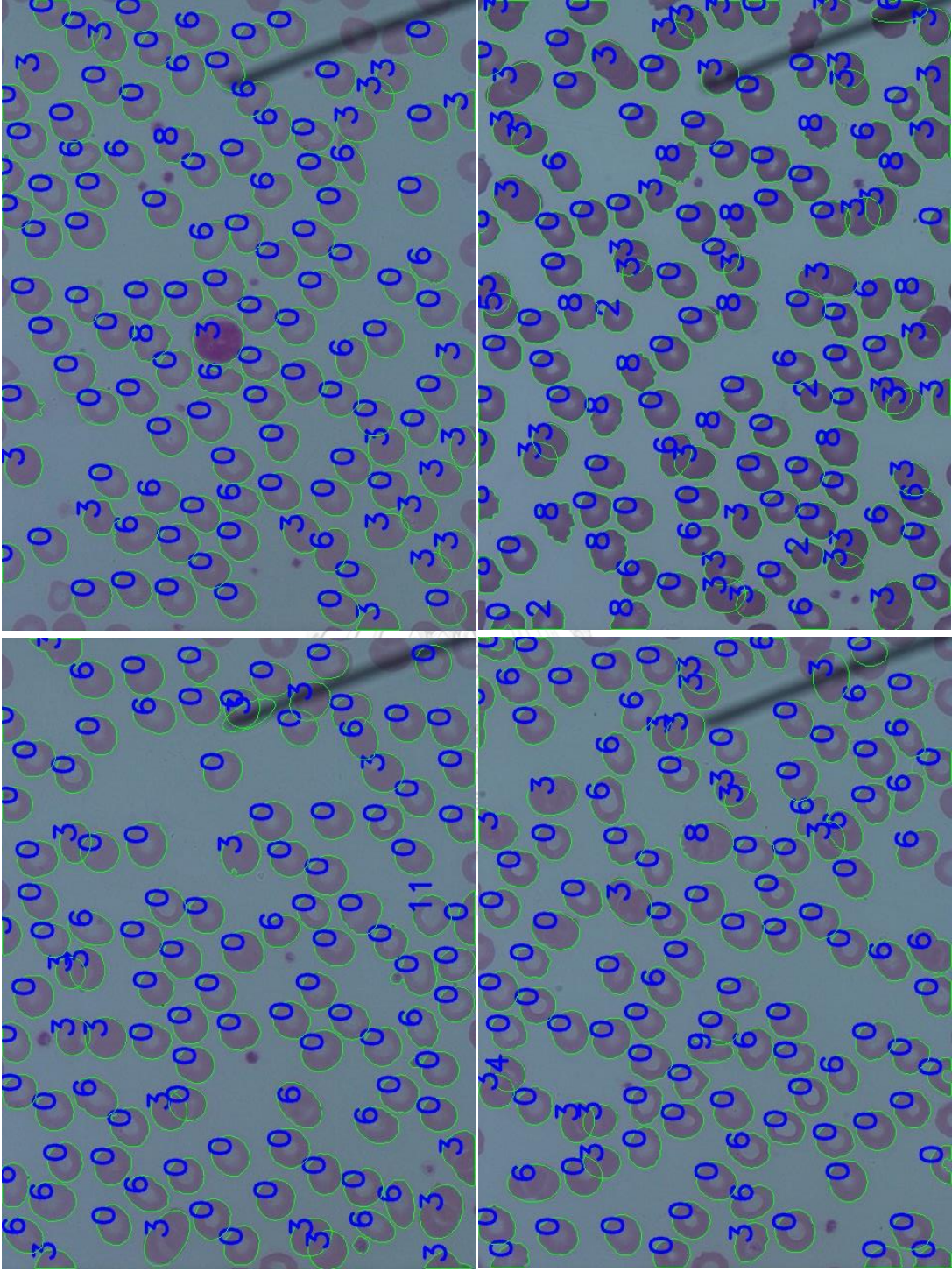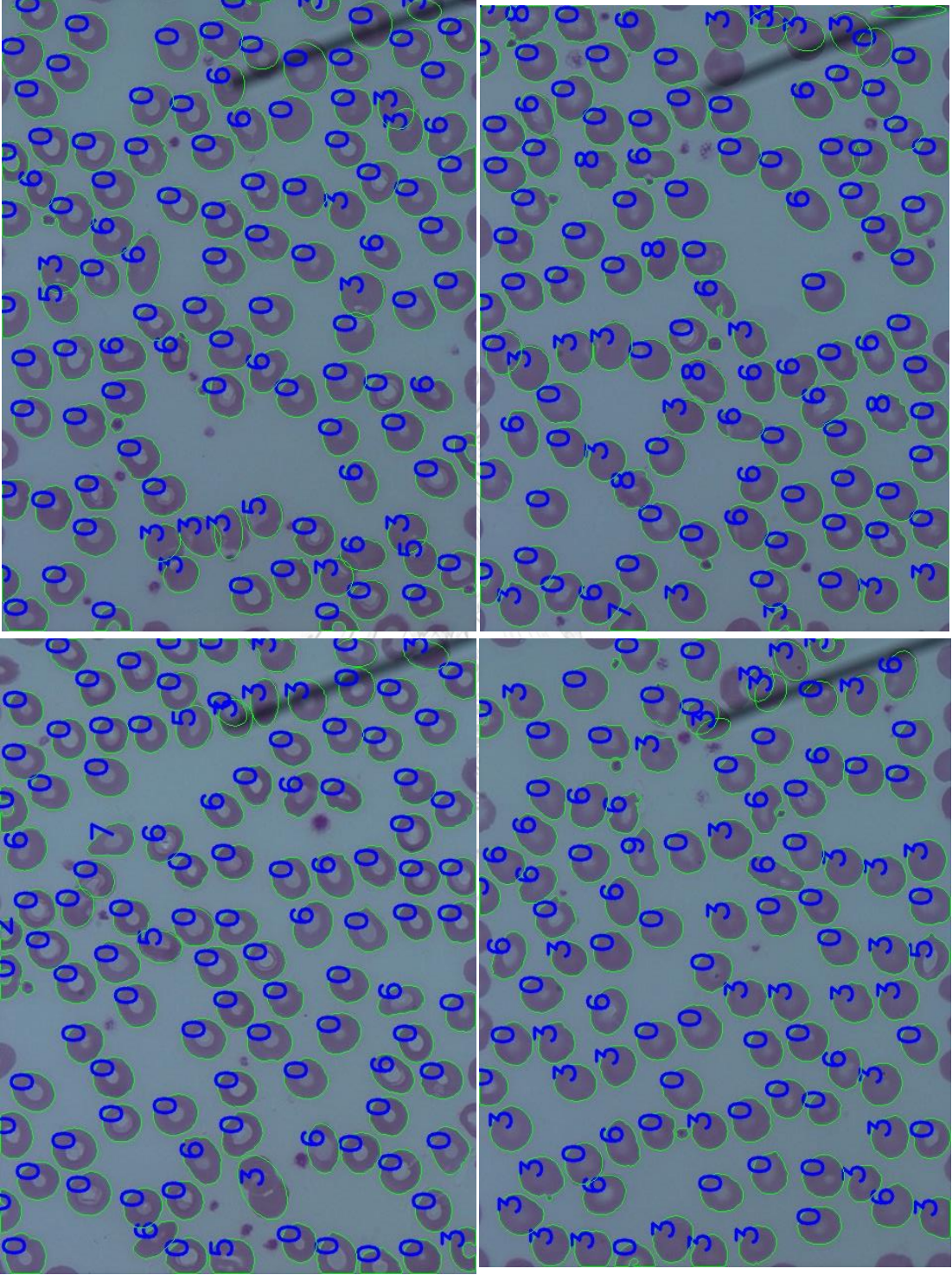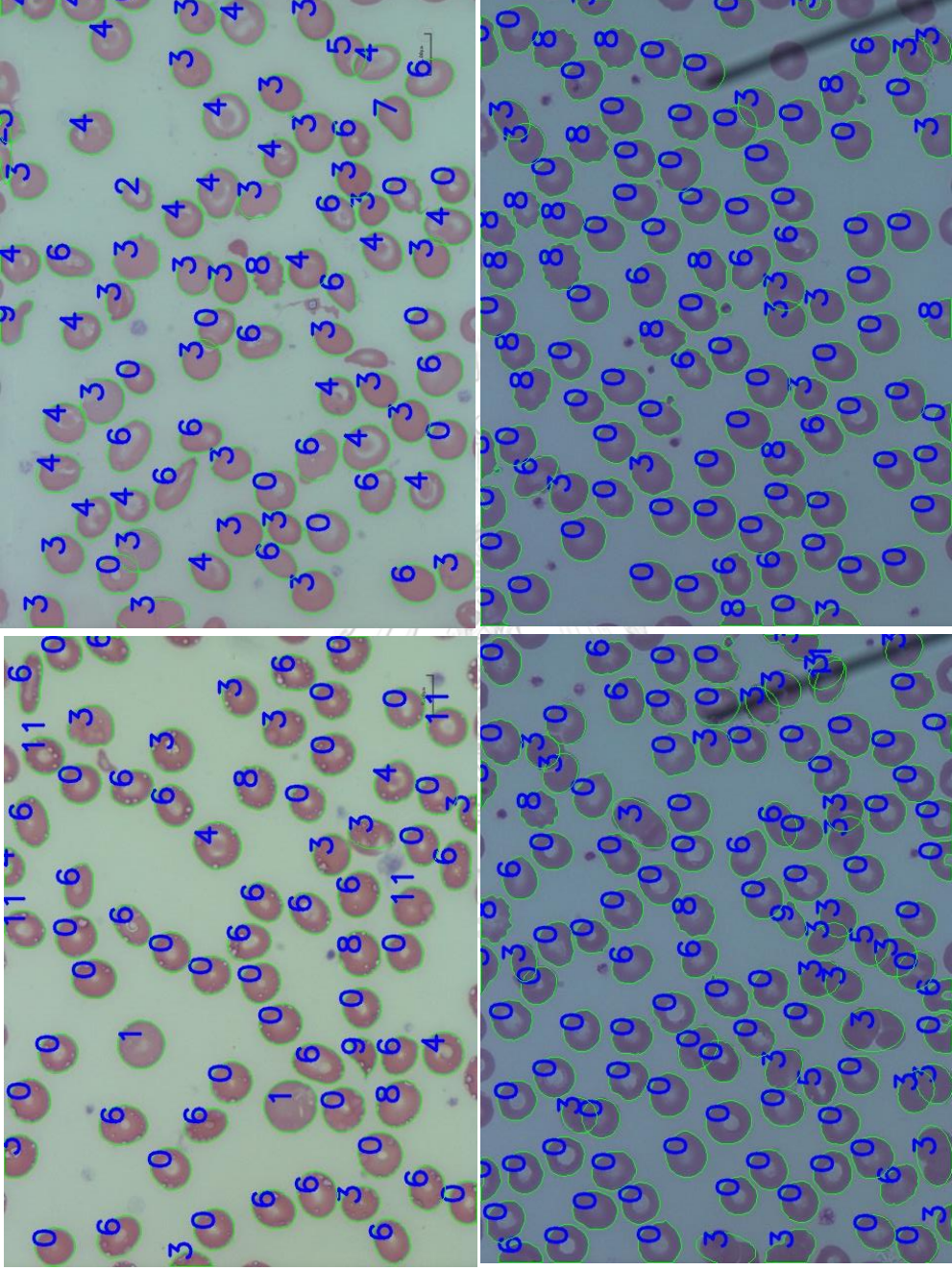
Figure 5-3 Samples of RBC segmentation and classification

5.3. RBC classification on other work comparisons

5.3.1. Comparison with (Wong et al., 2021)

(Wong et al., 2021) reported the results of using SVM and TabNet to classify the RBCs into 11 classes on the same dataset as used in this paper. They employed the SMOTE technique with cost-sensitive learning to handle the imbalanced dataset. The evaluation was done using F2-Score and the results show that the SVM outperforms the TabNet with 78.2% and 73.0% respectively. To compare with their work, we employed our methods, EfficientNet-B1 with augmentation, to classify 11 and 12 classes of RBCs on the same dataset. Our approach yields 88.62% and 87.91% F2-score respectively.

5.3.2. Comparison with Yale's dataset

Since each of researchers usually has their own datasets which are different in the number of classes and the number of samples, thus the method comparison is quite not straightforward. However, we found an available RBC dataset used in (Durant et al., 2017) provided by the Yale University School of Medicine. Their dataset contains 3,737 labeled RBCs with 10 classes including the overlapping cells. Durant et.al. used DenseNet (Huang et al., 2018) which has more than 150 layers. The reported accuracy was 0.9692 on the test set. Comparison on the Yale's dataset

To make a fair comparison, we employed our proposed method based on the EfficientNet-B1 without the overlapping cell separation. We also used five-fold cross validation for training because we do not know how the data was partitioned in the (Durant et al., 2017). Our result yields 0.9813 on the average accuracy on cross validation, and the highest and lowest cross validation accuracies are 0.9920 and 0.9733, respectively. Table 5-7 shows our average precision, recall, and F1-Score of five-fold cross validation on Yale's dataset. Table 5-8 shows confusion matrix for our

classifier based on EfficientNet-B1. There were only 6 wrong predicted results, as shown in Figure 5-4.

According to the comparison result on the same dataset, our proposed method outperforms the previous work done in (Durant et al., 2017) by yielding the higher accuracy. The overlapping cells were all correctly predicted in all five-fold cross validation which is quite obvious because the area of an overlapping cell is typically larger than other types of a single cell. Although accuracy gain using our model compared with the previous method is about 0.18% (7/3,737) which is not quite significant, but our model yields also better performance on both training and inference due to lots lower number of parameters.

Table 5-7 Average Precision, Recall, and F1-score of five-fold cross validation using our method on Yale's dataset

RBC Types	Precision	Recall	F1-score
Normal	0.995	0.985	0.990
Chinocyte	0.952	0.984	0.968
Dacrocyte	0.889	0.941	0.914
Schistocyte	0.974	0.949	0.961
Elliptocyte	0.889	0.941	0.914
Acanthocyte	0.848	0.933	0.889
Target cell	1.000	0.993	0.997
Stomatocyte	0.955	0.955	0.955
Spherocyte	0.958	0.958	0.958
Overlap	1.000	1.000	1.000

(a) **Predicted**: Dacrocyte

True class: Schistocyte

(b) **Predicted**: Schistocyte

True class: Dacrocyte

(c) **Predicted**: Schistocyte

True class: Echinocyte

(d) **Predicted**: Acanthocyte

True class: Schistocyte

(e) **Predicted**: Dacrocyte

True class: Elliptocyte

(f) **Predicted**: Spherocyte

True class: Normal
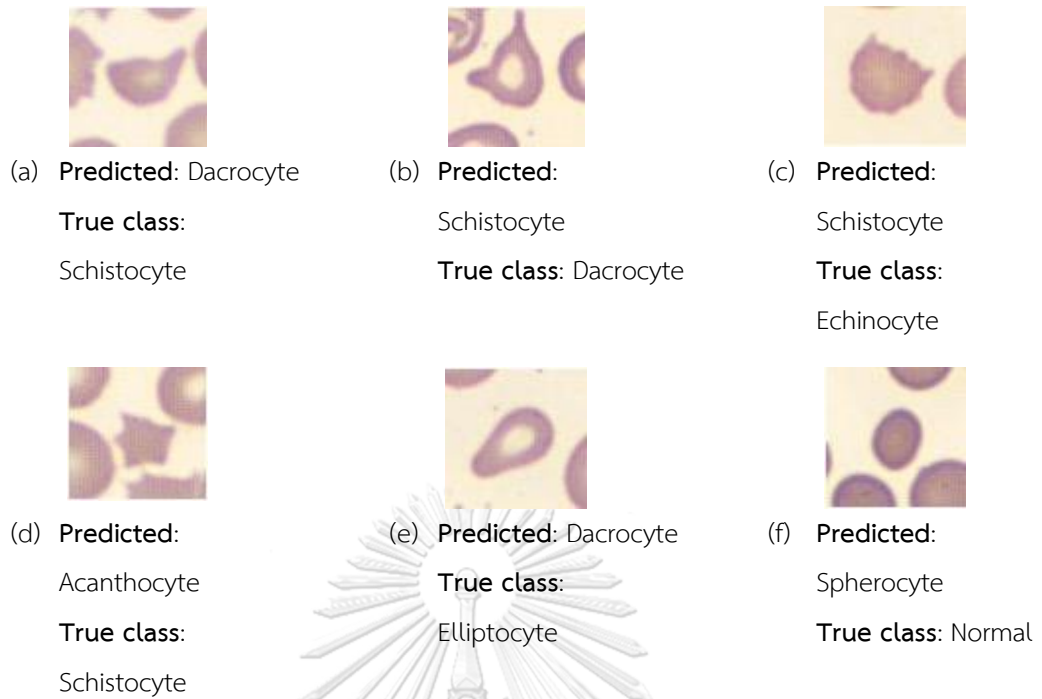
Figure 5-4 Among the 748 test images tested on EfficientNet-B1 using Yale's dataset, there were six misclassified images (a) - (f)

Table 5-8 Confusion matrix for our proposed method trained and tested on Yale's dataset

Predicted Class	True Class									
	Normal	Echinocyte	Dacrocyte	Schistocyte	Elliptocyte	Acanthocyte	Target cell	Stomatocyte	Spherocyte	Overlap
Normal	203	0	0	0	0	0	0	0	0	0
Echinocyte	0	63	0	0	0	0	0	0	0	0
Dacrocyte	0	0	16	1	1	0	0	0	0	0
Schistocyte	0	1	1	150	0	0	0	0	0	0
Elliptocyte	0	0	0	0	18	0	0	0	0	0
Acanthocyte	0	0	0	1	0	32	0	0	0	0
Target cell	0	0	0	0	0	0	145	0	0	0
Stomatocyte	0	0	0	0	0	0	0	22	0	0
Spherocyte	1	0	0	0	0	0	0	0	47	0
Overlap	0	0	0	0	0	0	0	0	0	46

Further cross dataset analysis was done with the EfficientNet-b1 model trained with our dataset but tested on the Yale's dataset. These two datasets have 8 identical RBC types that our dataset does not have the Acanthocyte and Overlap classes. In Table 5-9, the confusion matrix for the EfficientNet-B1 model trained on our dataset but tested on the Yale's dataset is shown. To test on different dataset, normalization process was done before classifying. The average accuracy was 0.7373 on 8 classes. 566 Normal RBCs was predicted wrong with Uncategorized class, which contains several RBC shapes. According to the incorrect Uncategorized class results, it can happen because many RBCs on Yale's dataset, even on the same types on our dataset, is not the same as on our dataset in some characteristic of RBCs.

The confusion matrix for the EfficientNet-B1 model trained on our dataset but tested on the Yale's dataset which excludes the Uncategorized class was shown for the analysis on the second best predicted of RBC types instead of the Uncategorized, as shown in Table 5-10. The average accuracy was 0.8062 on 8 classes. The result shows that the correct predicted normal class was huge increased. However, the incorrect results still have much more than the model trained on Yale's dataset.

To clarify the incorrect results, the misclassified images in Yale's dataset were observed, as shown in Figure 5-5. (a) – (d) are wrong predicted but it is quite reasonable because the images look similar to the predicted classes. In contrast, (e) – (g) are Schistocytes but the images only seem like the predicted class. The reason that our model shows wrong predicted results because the Schistocyte is a fragment of RBCs which cannot identify the characteristic of the Schistocyte.

82

Table 5-9 Confusion matrix for EfficientNet-B1 trained on our dataset and tested on Yale's dataset

| | True classes | | | | | | | | | |
Predicted classes	Normal	Echinocyte (Burr Cell)	Dacrocyte (Teardrop)	Schistocyte	Elliptocyte (Ovalocyte)	Target cell	Stomatocyte	Spherocyte	Acanthocyte	Overlap
Normal	76	0	0	0	0	0	0	0	0	0
Burr cell	0	260	0	4	0	0	0	0	70	0
Teardrop	5	1	83	200	5	0	0	1	3	0
Schistocyte	3	11	2	390	0	0	0	0	74	0
Ovalocyte	36	16	0	58	86	1	0	0	2	30
Target cell	6	0	0	7	0	701	0	0	0	0
Stomatocyte	2	0	0	0	0	0	73	3	0	0
Spherocyte	259	0	3	53	0	0	18	234	11	168
Macrocyte	2	0	0	0	0	0	0	0	0	0
Microcyte	44	2	0	9	0	3	1	0	0	0
Uncategorized	566	22	1	32	0	10	18	2	6	32
Hypochromia	13	2	0	6	0	11	0	0	0	0
Accuracy	7.51%	82.80%	93.26%	51.38%	94.51%	96.56%	66.36%	97.50%		

Table 5-10 Confusion matrix for EfficientNet-B1 trained on our dataset and tested on Yale's dataset (not included Uncategorized)

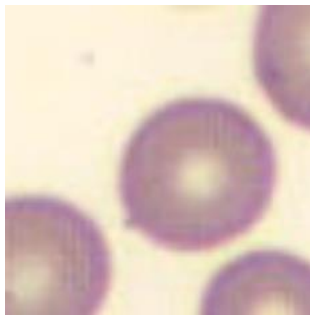| Predicted classes	True classes									
	Normal	Echinocyte (Burr cell)	Dacrocyte (Teardrop)	Schistocyte	Elliptocyte (Ovalocyte)	Target cell	Stomatocyte	Spherocyte	Acanthocyte	Overlap
Normal	412	0	0	0	0	0	1	0	0	0
Burr cell	0	280	0	4	0	0	0	0	72	0
Teardrop	13	1	84	202	5	0	0	1	3	0
Schistocyte	6	12	2	413	0	0	2	0	78	0
Ovalocyte	67	17	0	60	86	1	0	1	2	31
Target cell	9	0	0	7	0	711	0	0	0	1
Stomatocyte	9	0	0	0	0	0	84	4	0	0
Spherocyte	370	0	3	53	0	0	22	234	11	198
Macrocyte	5	0	0	0	0	0	0	0	0	0
Microcyte	90	2	0	12	0	3	1	0	0	0
Hypochromia	31	2	0	8	0	11	0	0	0	0
Accuracy	40.71%	89.17%	94.38%	54.41%	94.51%	97.93%	76.36%	97.50%		
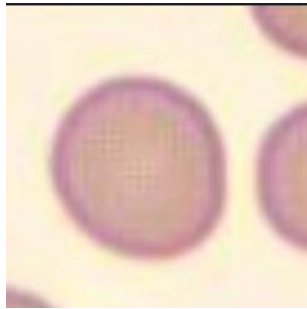
(a) True class: Normal

Predicted class: Spherocyte

(b) True class: Normal

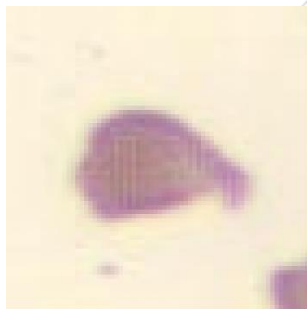Predicted class: Ovalocyte

(c) True class: Normal

Predicted class: Microcyte

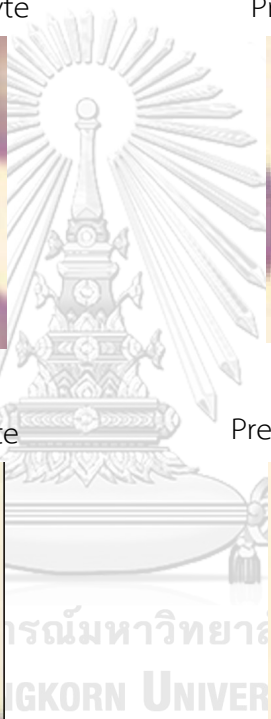(d) True class: Normal

Predicted class: Hypochromia

(e) True class: Schistocyte
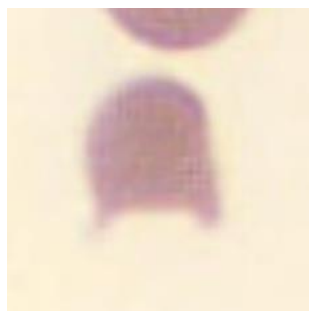
Predicted class: Teardrop

(f) True class: Schistocyte

Predicted class: Ovalocyte

(g) True class: Schistocyte

Predicted class: Spherocyte

Figure 5-5 Samples of misclassified images from the EfficientNet-B1 trained on our dataset and tested on Yale's dataset (not included Uncategorized)

6. Conclusion and Discussion

6.1. Conclusion

In this study, a method to segment RBCs is presented. The proposed method has the ability to separate overlapping cells based on concave points and classify RBCs into 12 classes. The process started from data collection with an application created for labeling RBCs. Color normalization, which reduced the color space and allowed the trained model to not be biased on color. Next, contour extraction was used to extract the RBC contour from the background. Then, overlapping cells were separated using a new method to find concave points and use direct ellipse fitting to estimate the shape of a single RBC. Lastly, classification using EfficientNet-B1 showed the best result with augmentation. Moreover, further analysis for handing an imbalanced dataset revealed that weight balancing can reduce the bias of a trained model on the majority classes.

6.2. Discussion

Many deep learning studies on RBCs still lack a standard public dataset to evaluate their performance. Our dataset has more samples and more types of RBCs than many previous studies, but it still requires to be improved for imbalanced problems.

For the method presented here, we used the EfficientNet model to classify the RBCs. However, the segmentation step is not a learning-based method, which is a trend that has shown better results in many specific computer vision areas. For RBC diagnose, only the number of RBCs and RBC types are important. The object detection method, which is provides bounding boxes and classes, can serve this. To train object detection for RBC images, all of RBCs are needed to label to make the best performance for the model. The manual labeling process may take much cost and time. Our work can use to do this labeling and classify with high accuracy for

these 12 RBC classes that is a starting point for end-to-end deep learning. However, RBC images are needed to be collected to solve the imbalanced problem and improve the performance.

REFERENCES

Abdulkarim, H., Razak, M. A. A., Sudirman, R., & Ramli, N. (2020). A deep learning AlexNet model for classification of red blood cells in sickle cell anemia. doi:10.11591/IJAI.V9.I2.PP221-228

Acharya, V., & Kumar, P. (2017, Sep. 2017). *Identification and red blood cell classification using computer aided system to diagnose blood disorders.* Paper presented at the 2017 International Conference on Advances in Computing, Communications and Informatics (ICACCI).

Ahmad, I., Abdullah, S. N. H. S., & Sabudin, R. Z. A. R. (2016, November 2016). *Geometrical vs spatial features analysis of overlap red blood cell algorithm.* Paper presented at the 2016 International Conference on Advances in Electrical, Electronic and Systems Engineering (ICAEES).

Aliyu, H. A., Razak, M. A. A., & Sudirman, R. (2019). Segmentation and detection of sickle cell red blood image. *AIP Conference Proceedings, 2173*(1), 020004. doi:10.1063/1.5133919

Alom, M. Z., Yakopcic, C., Taha, T. M., & Asari, V. K. (2018, July 2018). *Microscopic Blood Cell Classification Using Inception Recurrent Residual Convolutional Neural Networks.* Paper presented at the NAECON 2018 - IEEE National Aerospace and Electronics Conference.

Alzubaidi, L., Fadhel, M. A., Al-Shamma, O., Zhang, J., & Duan, Y. (2020). Deep Learning Models for Classification of Red Blood Cells in Microscopy Images to Aid in Sickle Cell Anemia Diagnosis. *Electronics, 9*(3), 427. doi:10.3390/electronics9030427

Batitis, V. M. E., Caballes, M. J. G., Ciudad, A. A., Diaz, M. D., Flores, R. D., & Tolentin, E. R. E. (2020, March 2020). *Image Classification of Abnormal Red Blood Cells Using Decision Tree Algorithm.* Paper presented at the 2020 Fourth International Conference on Computing Methodologies and Communication (ICCMC).

Cai, R., Wu, Q., Zhang, R., Fan, L., & Ruan, C. (2012, October 2012). *Red blood cell segmentation using Active Appearance Model.* Paper presented at the 2012

IEEE 11th International Conference on Signal Processing.

Chandrasiri, S., & Samarasinghe, P. (2014, December 2014). *Automatic anemia identification through morphological image processing.* Paper presented at the 7th International Conference on Information and Automation for Sustainability.

de Haan, K., Ceylan Koydemir, H., Rivenson, Y., Tseng, D., Van Dyne, E., Bakic, L., . . . Ozcan, A. (2020). Automated screening of sickle cells using a smartphone-based microscope and deep learning. *npj Digital Medicine, 3*(1), 1-9. doi:10.1038/s41746-020-0282-y

Delgado-Ortet, M., Molina-Borrás, A., Alférez, S., Rodellar, J., & Merino, A. (2020). A Deep Learning Approach for Segmentation of Red Blood Cell Images and Malaria Detection. *Entropy, 22*, 657. doi:10.3390/e22060657

Durant, T. J. S., Olson, E. M., Schulz, W. L., & Torres, R. (2017). Very Deep Convolutional Neural Networks for Morphologic Classification of Erythrocytes. *Clinical Chemistry, 63*(12), 1847-1855. doi:10.1373/clinchem.2017.276345

Fitzgibbon, A., & Fisher, R. (1995, 1995). *A Buyer's Guide to Conic Fitting.* Paper presented at the British Machine Vision Conference 1995.

Fitzgibbon, A., Pilu, M., & Fisher, R. B. (1999). Direct least square fitting of ellipses. *IEEE Transactions on Pattern Analysis and Machine Intelligence, 21*(5), 476-480. doi:10.1109/34.765658

Ford, J. (2013). Red blood cell morphology. *International Journal of Laboratory Hematology, 35*(3), 351-357. doi:10.1111/ijlh.12082

González-Hidalgo, M., Guerrero-Peña, F. A., Herold-García, S., Jaume-i-Capó, A., & Marrero-Fernández, P. D. (2015). Red Blood Cell Cluster Separation From Digital Images for Use in Sickle Cell Disease. *IEEE Journal of Biomedical and Health Informatics, 19*(4), 1514-1525. doi:10.1109/JBHI.2014.2356402

Gopakumar, G. P., Swetha, M., Siva, G. S., & Subrahmanyam, G. R. K. S. (2018). Convolutional neural network-based malaria diagnosis from focus stack of blood smear images acquired using custom-built slide scanner. *Journal of Biophotonics, 11*(3), e201700003. doi:10.1002/jbio.201700003

Habibzadeh, M., Krzyzak, A., Fevens, T., & Sadr, A. (2011, March 1, 2011). *Counting of RBCs and WBCs in noisy normal blood smear microscopic images.* Paper

presented at the Proc SPIE.

He, K., Zhang, X., Ren, S., & Sun, J. (2015). Deep Residual Learning for Image
Recognition. *arXiv:1512.03385 [cs]*.

Hegde, R. B., Prasad, K., Hebbar, H., & Sandhya, I. (2018). Peripheral blood smear
analysis using image processing approach for diagnostic purposes: A review.
Biocybernetics and Biomedical Engineering, 38(3), 467-480.
doi:10.1016/j.bbe.2018.03.002

Huang, G., Liu, Z., van der Maaten, L., & Weinberger, K. Q. (2018). Densely Connected
Convolutional Networks. *arXiv:1608.06993 [cs]*.

Johnson, J. M., & Khoshgoftaar, T. M. (2019). Survey on deep learning with class
imbalance. *Journal of Big Data, 6*(1), 1-54. doi:10.1186/s40537-019-0192-5

Kareem, S., Morling, R. C. S., & Kale, I. (2011, May 2011). *A novel method to count the
red blood cells in thin blood films.* Paper presented at the 2011 IEEE
International Symposium of Circuits and Systems (ISCAS).

Khashman, A. (2008). IBCIS: Intelligent blood cell identification system. *Progress in
Natural Science, 18*(10), 1309-1314. doi:10.1016/j.pnsc.2008.03.026

Krizhevsky, A., Sutskever, I., & Hinton, G. E. (2012, December 3, 2012). *ImageNet
classification with deep convolutional neural networks*.

Lee, H., & Chen, Y.-P. P. (2014). Cell morphology based classification for red cells in
blood smear images. *Pattern Recognition Letters, 49*, 155-161.
doi:10.1016/j.patrec.2014.06.010

Liang, Z., Powell, A., Ersoy, I., Poostchi, M., Silamut, K., Palaniappan, K., . . . Thoma, G.
(2016, December 2016). *CNN-based image analysis for malaria diagnosis.* Paper
presented at the 2016 IEEE International Conference on Bioinformatics and
Biomedicine (BIBM).

Lin, T.-Y., Goyal, P., Girshick, R., He, K., & Dollár, P. (2018). Focal Loss for Dense Object
Detection. *arXiv:1708.02002 [cs]*.

Long, J., Shelhamer, E., & Darrell, T. (2015). Fully Convolutional Networks for Semantic
Segmentation. *arXiv:1411.4038 [cs]*.

Mazalan, S. M., Mahmood, N. H., & Razak, M. A. A. (2013, December 2013). *Automated
Red Blood Cells Counting in Peripheral Blood Smear Image Using Circular*

Hough Transform. Paper presented at the Modelling and Simulation 2013 1st International Conference on Artificial Intelligence.

Nugroho, H. A., Akbar, S. A., & Murhandarwati, E. E. H. (2015, October 2015). *Feature extraction and classification for detection malaria parasites in thin blood smear.* Paper presented at the 2015 2nd International Conference on Information Technology, Computer, and Electrical Engineering (ICITACEE).

Parab, M. A., & Mehendale, N. D. (2020). Red blood cell classification using image processing and CNN. *bioRxiv*, 2020.2005.2016.087239. doi:10.1101/2020.05.16.087239

Pasupa, K., Vatathanavaro, S., & Tungjitnob, S. (2020). Convolutional neural networks based focal loss for class imbalance problem: a case study of canine red blood cells morphology classification. *Journal of Ambient Intelligence and Humanized Computing*. doi:10.1007/s12652-020-01773-x

Qiu, W., Guo, J., Li, X., Xu, M., Zhang, M., Guo, N., & Li, Q. (2019). Multi-label Detection and Classification of Red Blood Cells in Microscopic Images. *arXiv:1910.02672 [cs, eess, stat]*.

Rahman, S., Azam, B., Khan, S. U., Awais, M., Ali, I., & ul Hussen Khan, R. J. (2021). Automatic identification of abnormal blood smear images using color and morphology variation of RBCS and central pallor. *Computerized Medical Imaging and Graphics, 87*, 101813. doi:10.1016/j.compmedimag.2020.101813

Rakshit, P., & Bhowmik, K. (2013). Detection of Abnormal Findings in Human RBC in Diagnosing Sickle Cell Anaemia Using Image Processing. *Procedia Technology, 10*, 28-36. doi:10.1016/j.protcy.2013.12.333

Ren, S., He, K., Girshick, R., & Sun, J. (2016). Faster R-CNN: Towards Real-Time Object Detection with Region Proposal Networks. *arXiv:1506.01497 [cs]*.

Ritter, N., & Cooper, J. (2007, 2007). *Segmentation and Border Identification of Cells in Images of Peripheral Blood Smear Slides*.

Romero-Rondón, M., Sanabria-Rosas, L., Bautista-Rozo, L., & Mendoza, A. (2016). Algorithm for detection of overlapped red blood cells in microscopic images of blood smears. *Dyna (Medellin, Colombia), 83*, 188-195. doi:10.15446/dyna.v83n198.47177

Sadafi, A., Radolko, M., Serafeimidis, I., & Hadlak, S. (2018, December 2018). *Red Blood Cells Segmentation: A Fully Convolutional Network Approach.* Paper presented at the 2018 IEEE Intl Conf on Parallel Distributed Processing with Applications, Ubiquitous Computing Communications, Big Data Cloud Computing, Social Computing Networking, Sustainable Computing Communications (ISPA/IUCC/BDCloud/SocialCom/SustainCom).

Shakarami, A., Menhaj, M. B., Mahdavi-Hormat, A., & Tarrah, H. (2021). A fast and yet efficient YOLOv3 for blood cell detection. *Biomedical Signal Processing and Control, 66*, 102495. doi:10.1016/j.bspc.2021.102495

Sharma, V., Rathore, A., & Vyas, G. (2016, August 2016). *Detection of sickle cell anaemia and thalassaemia causing abnormalities in thin smear of human blood sample using image processing.* Paper presented at the 2016 International Conference on Inventive Computation Technologies (ICICT).

Simonyan, K., & Zisserman, A. (2015). Very Deep Convolutional Networks for Large-Scale Image Recognition. *arXiv:1409.1556 [cs]*.

Soltanzadeh, R., & Rabbani, H. (2010, October 2010). *Classification of three types of red blood cells in peripheral blood smear based on morphology.* Paper presented at the IEEE 10th INTERNATIONAL CONFERENCE ON SIGNAL PROCESSING PROCEEDINGS.

Tan, M., & Le, Q. V. (2020). EfficientNet: Rethinking Model Scaling for Convolutional Neural Networks. *arXiv:1905.11946 [cs, stat]*.

Tomari, R., Zakaria, W. N. W., Jamil, M. M. A., Nor, F. M., & Fuad, N. F. N. (2014). Computer Aided System for Red Blood Cell Classification in Blood Smear Image. *Procedia Computer Science, 42*, 206-213. doi:10.1016/j.procs.2014.11.053

Tyas, D. A., Ratnaningsih, T., Harjoko, A., & Hartati, S. (2017, 2017). *The Classification of Abnormal Red Blood Cell on The Minor Thalassemia Case Using Artificial Neural Network and Convolutional Neural Network.*

Wong, A., Anantrasirichai, N., Chalidabhongse, T. H., Palasuwan, D., Palasuwan, A., & Bull, D. (2021). Analysis of Vision-based Abnormal Red Blood Cell Classification. *arXiv:2106.00389 [cs]*.

Xu, M., Papageorgiou, D. P., Abidi, S. Z., Dao, M., Zhao, H., & Karniadakis, G. E. (2017). A

deep convolutional neural network for classification of red blood cells in sickle
cell anemia. *PLOS Computational Biology, 13*(10), e1005746.
doi:10.1371/journal.pcbi.1005746

Zhang, M., Li, X., Xu, M., & Li, Q. (2017). Image Segmentation and Classification for Sickle
Cell Disease using Deformable U-Net. *arXiv:1710.08149 [cs, q-bio]*.

VITA

NAME   Korranat Naruenatthanaset

DATE OF BIRTH   28 November 1994

PLACE OF BIRTH   Mahasarakham

INSTITUTIONS ATTENDED Chulalongkorn University

HOME ADDRESS   2 Soi 9, Srimahasarakham road, Talad, Muang,

Mahasarakham